INTERNATIONAL ATOMIC ENERGY AGENCY
UNITED NATIONS EDUCATIONAL, SCIENTIFIC AND CULTURAL ORGANIZATION
INTERNATIONAL CENTRE FOR THEORETICAL PHYSICS
I.C.T.P., P.O. BOX 586, 34100 TRIESTE, ITALY, CABLE: CENTRATOM TRIESTE

SMR.703 - 21

WORKING PARTY ON
MECHANICAL PROPERTIES OF INTERFACES

23 AUGUST - 3 SEPTEMBER 1993

"Dynamic Strain Ageing (DSA) and Grain Boundaries - Some Interesting Results of Hall-Petch Analysis in DSA Regime"

Placid RODRIGUEZ
Indira Gandhi Centre for Atomic Research
Kalpakkam 603 102
Tamilnadu
INDIA

DYNAMIC STRAIN AGEING (DSA) AND GRAIN BOUNDARIES - SOME INTERESTING RESULTS OF HALL-PETCH ANALYSIS IN DSA REGIME

PLACID RODRIGUEZ
Director
Indira Gandhi Centre for Atomic Research
Kalpakkam 603 102
Tamilnadu, India

Prepared for presentation at the Working Party on: MECHANICAL PROPERTIES OF INTERFACES, 23 August - 3 September 1993, International Centre for Theoretical Physics, Trieste, Italy.

1. INTRODUCTION

In many solid solution alloys, the phenomenon of serrated flow (or Portevin - Le Chatelier effect, PLE after Portevin and Le Chatelier 1923 [1]) which begins after a finite amount of critical strain ϵ_c has been explained based on the dynamic interaction between solute atoms and mobile dislocations, known as dynamic strain ageing (DSA) and has been the subject of several reviews [2-4]. In a recent review, Rodriguez [4] has made an assesment of the current understanding of the phenomenon of serrated yielding and has emphasised that serrations represent only one of the manifestations of DSA. The other manifestations of DSA include the work hardening peak, the flow stress peak or plateau, the ductility minimum and the negative strain rate sensitivity of flow stress.

In the literature, majority of the studies have been devoted to understanding the effects of strain rate, temperature and chemical composition on various aspects of DSA. The studies concerning the effect of grain size on DSA have been very few. These studies pertain to Al-Mg [5,6], Cu-Zn [7,8] and Cu-Sn [9,10] alloys and have shown that grain size has a significant effect on the nature and occurrence of serrated yielding. Though the phenomenon of DSA has been reported to occur in austenitic stainless steels [11-15], in the range of temperatures from 473 to 973 K, the investigations concerning the role of grain size on DSA have not been attempted till recently in this material which is widely used in liquid metal fast breeder reactors (LMFBRs). The situation is same for another important material Zirconium, an alloy of which is used in thermal nuclear reactors. This paper reports the results pertaining to grain size effects on DSA in an AISI type 316 stainless steel at elevated temperatures and in Zr at low and ambient temperatures. Further the results on the effect of thermal ageing on

serrated flow in an AISI 316 austenitic stainless steel and some results on the role of grain size on DSA in low cycle fatigue in a type 304 stainless steel are presented. The effect of grain size on DSA in a type 316 stainless steel is a part of the detailed investigation on the influence of grain size on the flow and fracture behaviour at elevated temperatures [16]. The results pertaining to Zr are also a part of a systematic study on the low temperature deformation behaviour in hard hcp metals [17].

This paper discusses the results of phenomenon of DSA and grain size effects from two different approaches. For the results on type 316 stainless steel, the DSA analysis pertains to the analysis of charateristics of serrated flow and other manifestations such as work hardening peak, flow stress plateau and the peak in the variation of Hall - Petch slope with temperature. Whereas the results on Zr include the observed anamolies in the parameters of thermally activated strain rate analysis (TASRA); for eg., the anamolous behaviour of activation energy and activation area. Before presenting the results on the role of grain size (grain boundaries) on DSA, it is in order to introduce the phenomenon and various models of DSA and serrated flow and a brief account on grain boundary strengthening.

2. SERRATED YIELDING

The detailed account of phenomenology of serrated flow, various physical processes that can cause serrated flow and types of serrations have been described in a recent review by Rodriguez [4]. It should be mentioned that the serrations or load drops appear on a stress - strain curve when the plastic strain rate exceeds the imposed strain rate. As the plastic strain rate is dependent on mobile dislocation density ρ_m

and average dislocation velocity $\bar{v}$ ($\dot{\epsilon} = \rho_m b \bar{v}$, where b is the Burger's vector); the serrations occur whenever there is an instantaneous increase in ρ_m or in $\bar{v}$ or in both.

2.1 Nature of Serrations

So far five types of serrations due to DSA viz. A, B, C, D and E have been identified [4, 18-21]. The characteristics of different types of serrations and the experimental conditions that produce them are breifly given below.

i) Type A serrations are termed as locking serrations. Each serration corresponds to the initiation of a Lüders Band, which then propagates along the length of the specimen. Further deformation occurs by the initiation of a new Lüders band, as evidenced by the rapid rise and discontinuos drop in flow stress. The strain ageing occurs very rapidy behind the propagating Lüders band and this type of serrtaions occur at low and intermediate temperatures, and at high strain rates in the DSA regime.

ii) Type B serrations are fine scale oscillations about the general level of the stress - strain ($\sigma - \epsilon$) curve and are due to discontinuos band propagation. The band hops from one position to another position and each hop corresponds to one serration. Type B often develops from those of type A [Fig. 1 inset] or occur at the onset of serrated yielding at high temperatures and lower strain rates.

iii) Type C serrations are yield drops that occur below the general level of the $\sigma - \epsilon$ curve and are termed as unlocking serrations. They occur at higher temperatures and lower strain rates than in the case of type A and B serrations.

iv) Type D are plateaus in the $\sigma - \epsilon$ curve due to band propagtion similar to Lüders band with no work hardening or strain gradient ahead of the moving band front.

v) Type A can change over to type E serrations at high strain rates and type E are similar to type A, but with little or no work hardening during band propagation.

It is important to mention that whenever mixed serrations appear on a $\sigma - \epsilon$ curve, careful and systematic analysis needs to be carried out [22-24]. A new type called "F type" serrations also have been reported in a 15Cr-15Ni Ti modified austenitic stainless steel [25].

2.2 Theories of DSA

The discussion is restricted to substitutional alloys which require a certain amount of critical strain ϵ_c for the onset of serrated flow. The value of ϵ_c is dependent on both strain rate $\dot{\epsilon}$ and temperature T (Fig. 2). At low and intermediate temperatures and at high strain rates (i.e. for type A or B), ϵ_c increases with increasing $\dot{\epsilon}$ and decreasing T. This is referred to as normal PL effect. Whereas at high temperatures and low strain rates (i.e . for type C), ϵ_c increases with increasing T and decreasing $\dot{\epsilon}$ (inverse PL effect). Any theory or model of DSA for serrated flow should account for the characteristics of serrations and for the influence of T and $\dot{\epsilon}$. While the understanding of type C unlocking serrations (inverse PL effect) has been very poor, most of the theoretical models based on DSA have been sucessful in explaining the normal PL effect. Mainly there are two models based on DSA; i.e. Vacancy or friction model [26-28] and the strain hardening or the forest model [29]. The important difference is in the interpretation of ϵ_c ; the latter model does not rely on the deformation induced vacancies, instead assumes a dislocation arrest

model in which sloute atoms diffuse along dislocations at forest intersections. An introduction of the vacancy model of DSA is necessary before understanding how the grain size effect is incorporated in the equation relating ϵ_c , $\dot{\epsilon}$ and T.

2.2.1 Vacancy model

In this section the theories of DSA after Cottrell [26] and McCormick [27] are discussed. The difference between the two models is the way in which DSA is assumed to occur. In the Cottrell theory, the mobile sloutes are assumed to interact with quasi - viscously moving dislocations; whereas the McCormick model in accordance with the idea advanced by Sleeswyk [30], considers that the ageing of dislocations would take place during the waiting time of dislocations temporarily arrested at discrete obstacles, rather than during their actual motion.

Cottrell theory

Before discussing the Cottrell theory of DSA, a brief description on dislocation - solute interaction is given. The possiblity of stress relief by solute migration was first suggested by Gorsky [31]. Cottrell [32,33] first considered the elastic interaction between a spherical atom and a stationary positive edge dislocation and this interaction relieves the hydrostatic stresses round an edge dislocation. The interaction or the binding energy is $U = \frac{A \sin\theta}{r}$, where r and θ are the polar co-ordinates of the solute atom measured from the dislocation and A is a parameter which depends on the elastic constants, volume change caused by the solute atom and the strength of the dislocation. This equation breaks down at the core of dislocation. The solute atom can interact with screw dislocations, if it produces non - spherical

distortion to relieve shear stresses. Such sloute - dislocation interactions cause the segregation of solutes round stationary dislocation with an equilibrium concentration $C = C_o \exp(-U/kT)$, where C_o is the average concentration of solutes, U is the binding energy and k is Boltzman constant. This expression of Maxwellian distribution is no longer valid for $U_{max} >> kT$. Under an external force, the dislocation surrounded by solute atmosphere can still move, if the atmosphere moves with it, although lagging behind. Cottrell and Jawson [34] developed a quantitative theory for the interaction of solute with positive edge dislocation, with the assumption that the solution is dilute and the interaction is weak. They suggested that the non-symmetry of the distribution of solute atoms round a moving dislocation (Fig. 3) would cause a perturbation force to act on dislocation opposing its motion; this force can be regarded as a viscous drag which increases with the speed of dislocation thereby allowing a steady motion of dislocation. Thus there exists a critical velocity above which the motion is unstable and the dislocation moves too fast to posses the solute atmosphere (Fig. 4).

The Cottrell model [26] of DSA attempts to determine the conditions that control the onset of serrations, by assuming that serrations appear when dislocation velocity becomes large enough to exceed the critical drag stress. Thus solute atmospheres form about and are dragged along by dislocations moving at less than the critical velocity v_c given by

$$v_c = \frac{4D}{l} \qquad \ldots\ldots(1)$$

where D is the solute diffusion coefficient, l the effective radius of

the atmosphere which is equal to $U_m b/kT$. Since above this velocity the stress decreases with increase in the dislocation velocity, it is logical to conclude that v_c represents a critical condition for the appearance of serrations on a $\sigma - \epsilon$ curve. Therefore there exists a critical $\dot{\epsilon}$ given by

$$\dot{\epsilon} = \phi \rho_m b v_c = \frac{4 \phi \rho_m b D}{l} \qquad .....(2)$$

where ϕ is a schmid orientation factor. Further, to account for the mobility of solutes at low temperatures at which DSA is observed, the contribution of vacancies generated during deformation was first suggested by Cottrell [26]. Thus in substitutional alloys, the increase in vacancy concentration C_v and decrease in dislocation velocity which during straining allow DSA to occur after a critical amount of strain ϵ_c has been acheived. Equation 2 may be rewritten as

$$\dot{\epsilon} = \frac{4 \phi b \rho_m C_v D_o \exp(-Q_m/kT)}{l} \qquad .....(3)$$

where D_o is the diffusion frequency factor, Q_m the effective activation energy for solute migration is equal to $(E_m - B)$, where E_m and B are activation energy for vacancy diffusion and solute - vacancy binding energy respectively. The strain dependence of strain induced vacancy concentration which exceeds the thermal equilibrium concentration of vacancies is expressed [36,37] as

$$C_v = K \epsilon^m \qquad .....(4)$$

where K and m are constants. The variation of ρ_m with ϵ is expressed as

$$\rho_m = N \epsilon^{\beta} \qquad .....(5)$$

where N and β are constants. This variation of ρ_m with ϵ was first incorporated by Ham and Jaffrey [38] to explain the observed value for the exponent in the $\ln \dot{\epsilon}$ Vs. $\ln \epsilon_c$ plot, determined by Russel [18] for Cu-Sn alloys. From equations (3),(4) and (5), the ϵ_c can be written as

$$\epsilon_c^{(m+\beta)} = \frac{l \dot{\epsilon} \exp(Q_m/kT)}{4 \phi b N K D_o} \qquad .....(6)$$

or in a simplified form as

$$\epsilon_c^{(m+\beta)} = K_1 \dot{\epsilon} \exp(Q_m/kT) . \qquad .....(7)$$

While Cottrell theory is able to predict both the $\dot{\epsilon}$ and T dependence of ϵ_c, it fails when it comes to predicting ϵ_c value itself. This led McCormick [27] to propose an alternative model following an idea advanced by Sleeswyk; McCormick as well as subsequent models integrate the Cottrell theory with the theory of thermally activated deformation processes.

McCormick model

In this alternative approach it is assumed that the motion of a dislocation in its slip plane is a discontinuous process and during deformation a mobile dislocation spends most of its time trying to

surpass the discrete obstacles. Once the obstacle is surpassed possibly with the help of thermal activation, the dislocation segment jumps at a high velocity to the next obstacle. It is important to note that the ageing or the interaction between mobile dislocations and diffusing solute atoms mainly occurs during the time the dislocation is waiting in front of the obstacles. If the diffusion coefficient is high enough to saturate the temporarily arrested dislocation during the waiting time with the solute atmosphere, serrated yielding will start. Such a process leads to an average velocity.

$$\bar{v} = \frac{L}{(t_w + t_f)} \qquad \ldots\ldots(8)$$

where L is the average distance between the obstacles, t_f is the mean time of flight between the obstacles and t_w is the mean time the dislocation waits for thermal activation. Specifically McCormick assumes that serrations appear on $\sigma - \epsilon$ curve when t_w becomes equal to t_a, the time needed to age or lock the arrested dislocation. When t_w is less than t_a at the start of plastic deformation, the $\sigma - \epsilon$ curve is continuous. But t_w increases and t_a decreases during straining and at a critical strain t_w becomes equal to t_a. Further $t_w >> t_f$ and the critical velocity v_c for the appearance of serrated flow becomes

$$v_c = \frac{L}{t_w} = \frac{L}{t_a} \; . \qquad \ldots\ldots(9)$$

McCormick also assumes a Cottrell - Bilby [33] time to the two thirds power law valid for elastic solute-dislocation interactions and for short ageing times

$$t_a = \left(\frac{C_1}{\alpha C_o}\right)^{3/2} \left(\frac{kT\, b^2}{3 U_m D}\right) \qquad \ldots\ldots(10)$$

where C_1 is the local solute concentration that the dislocation "sees", C_o is the original concentration of solute in the alloy, α is a constant equal to about 3 and U_m is the maximum solute - dislocation interaction energy. Assuming the dependence of C_v and ρ_m with ϵ, the McCormick model leads to a critical strain equation for a substitutional solute of the form

$$\epsilon_c^{(m+\beta)} = \left(\frac{C_1}{\alpha C_o}\right)^{3/2} \frac{\dot{\epsilon}\, kT\, b \exp(Q_m/kT)}{3\phi N K U_m D_o L} \; . \qquad \ldots\ldots(11)$$

Reed-Hill [39] expressed the comparison between McCormick and Cottrell theory as

$$\epsilon_{c\,McCormick}^{(m+\beta)} = \frac{4}{3}\left(\frac{C_1}{\alpha C_o}\right)^{3/2}\left(\frac{kT}{U_m}\right)\left(\frac{b}{l}\right)\left(\frac{b}{L}\right) \cdot \epsilon_{c\,Cottrell}^{(m+\beta)} \; . \qquad \ldots\ldots(12)$$

Using the parameter values as suggested by McCormick, i.e. $l = 10\ b$ $U_m = 0.5$ eV, $L = 10^{-5}$ Cm, $C_1 = 1$ and assuming kT is about 1/30 eV at room temperature, equation (12) becomes

$$\epsilon_{c\,McCormick}^{(m+\beta)} = \frac{6.8 \times 10^{-6}}{C_o^{3/2}}\, \epsilon_{c\,Cottrell}^{(m+\beta)} \; . \qquad \ldots\ldots(13)$$

substituting $C_o = 10^{-1}$ and $(m+\beta) = 2$ which are reasonable values for the systems investigated by McCormick and many others, one obtains according to McCormick model ϵ_c about 10^{-2} times that predicted by Cottrell theory. Thus McCormick theory predicts ϵ_c accurately. Moreover the solute drag model of cottrell does not predict the effect of composition on ϵ_c or on DSA. The simplified version of McCormick equation for ϵ_c can be given as

$$\epsilon_c = K_2 \dot{\epsilon}^{(m+\beta)} \exp(Q_m/kT) \quad \text{.....(14)}$$

For DSA due to interstitials solutes where m = 0, the equation [14] reduces to

$$\epsilon_c = K_2' \dot{\epsilon}^{\beta} \exp(Q_m/kT) \quad \text{.....(15)}$$

Generally in DSA involving substitutional solutes, values of $(m+\beta)$ between 2 and 3 have been obtained whereas for DSA due to interstitial solutes, $(m+\beta)$ i.e. β lies between 0.5 and 1 [4,40].

2.3 Other Approaches of DSA

The model developed by McCormick does not treat the other aspects of DSA such as; yield stress plateau, abnormal and rate dependent work hardening and the negative strain rate sensitivity (SRS). Van den Beukel [28] retains the approach of Sleeswyk and McCormick; i.e. the ageing of dislocations occur during their arrest and the phenomenological expressions for strain dependence of C_v and ρ_m. The significant contribution is that the DSA problem is treated following the concepts of thermally activated strain rate equation, where the activation enthalpy is assumed to depend on both the effective stress and the local solute concentration near the dislocation. Further this local concentration being dependent on D and t_w, and using phenomenological equations for C_v and ρ_m with ϵ, critical strain ϵ_c is interpreted as the strain at which the SRS becomes negative. It was first shown by Penning [41] that the inhomogeneous deformation as observed in PLE can be explained elegantly by assuming the negative SRS

in finite interval of strain rates. It should be mentioned that serrated yielding is due to the start of inhomogeneous deformation [42].

In an alternative strain hardening model, Mulford and Kocks [29], describe the SRS in terms of the flow stress σ which is the sum of two components - the friction stress σ_f and the dislocation flow stress σ_d; solute mobility affects σ_d, the strain hardening component of the flow stress. They contend that the rate sensitivity of σ_d is negative from the beginning; after some critical strain it dominates and renders the total rate sensitivity negative; which in turn causes serrated flow. This interpretation of critical strain does not rely on the production of vacancies for explaining the onset of serrated flow, instead it assumes the diffusion of solute atoms along dislocations at forest intersections. In a joint paper, Van den Beukel and Kocks [43] have arrived at a unified approach which enables the negative SRS to arise as a consequence of the influence of solute mobility on both σ_f (by decreasing the obstacle spacing along the dislocation) and σ_d (by increasing the strength of dislocation junctions). Recently, a treatment based on elementary strain theory which is neutral to both friction and forest models of DSA has been discussed by Kubin and Estrin [44].

Some objections [29,45,46] raised against vacancy model have been defended by Van den Beukel [40]. Recently the role of strain induced vacancies in serrated flow is discussed for a 15Cr-15Ni Ti modified austenitic stainless steel [24]. Though there is no consensus on the choice of the model for DSA, the vacancy model can not be rejected as it accounts for the differences observed in the ϵ_c Vs. $\dot{\epsilon}$ behaviour between interstitial and substitutional alloys.

Suggestions have also been made that serrated yielding could be considered as a manifestation of chaotic behaviour and an another example of a dissipative structure [47, 48], or as an example of a catastrophe in plastic deformation [49] arising from negative resistance feature, or due to modulations in order encountered by moving dislocations [50]. It has been suggested by Weertman [51] that the PLE occurs as a result of an instability of dislocations in going back and forth between a slow moving state and a fast moving state due to dynamic frictional stress drops; earthquakes are merely the PLE in a sample whose dimensions happen to have a grand scale. Mention should also be made of attempts to understand some of the features of DSA (negative SRS, work hardening and deformation by band propagation) through dry friction models [52, 53]. Thus in all the models negative SRS is the most crucial factor for describing PLE and DSA.

Though the vacancy models rationalize the onset of serration in particular and DSA in general as far as locking serrations are concerned, the explanation regarding type C unlocking serrations has been very poor. It is believed that in the inverse PLE region, the diffusion rates are high enough for dislocations to be aged from the start of deformation and type C serrations appear to be due to break away of these aged dislocations [54]. It has been suggested [44] that unlocking serrations are connected with precipitation before and during the test. Hayes [55] and Hayes and Hayes [56] carried out systematic investigations in AISI 1020, 2.25 Cr - 1 Mo, Inconel 718 and Inconel 600 to relate the strain for disappearance of serrations with $\dot{\epsilon}$ and T. They have shown that the disappearance of serrations from the flow curve occurs in the high temperature regime by either a progressively longer strain to the onset of serrations (a critical strain delay mechanism)

or by a progressively smaller strain to the disappearance of serrations (disappearance off the end of flow curve). In the former case, carbon diffusing down the dislocation line to a precipitate sink is suggested as the mechanism; whereas in the latter case, carbon reacting with a carbide-forming species on the dislocation line is responsible for the disppearance of serrations. Thus the important conclusion from their studies is that the disappearance is generally related to precipitation mechanism and the disappearance of serrated flow would occur when a balance is reached between the growth of carbon atmosphere and its depletion due to reaction between substitutional (carbide forming) atoms in the atmosphere. In this context, it has been suggested that the occurrence of type C serrations could be regarded as a precursor to the precipitation and disappearance of serrations [24].

2.4 Other Manifestations of DSA

It has been mentioned earlier that serrations represent only one of the manifestations of DSA. In Fig. 5 the various other anomalies associated with DSA are illustrated schematically [4]. These include a) a peak in the variation of flow stress with temperature, b) a peak in the variation of work hardening $\theta = \frac{\Delta\sigma}{\Delta\epsilon}$ with temperature, c) a peak in the variation of the Hall - Petch slope K_ϵ with temperature, d) a minimum in the variation of ductility with temperature and e) a minimum in the strain rate sensitivity $\gamma = \frac{\Delta\sigma}{\Delta \ln \dot{\epsilon}}$, with γ going negative in the temperature region of serrated flow. The variation of γ with σ and ϵ at different temperatures are also shown in Fig. 5. The types of serrations normally observed in the different temperature regimes are also indicated.

2.5 Anomalies in Thermally Activated Strain Rate Analysis (TASRA) parameters due to DSA

The detailed and systematic investigation [17] on low temperature deformation behaviour of hard hcp metals has revealed that the controversial aspect in these is the anomalous variation of experimentally determined activation energy with temperature. A novel experimental technique devised by Rodriguez [17,57,58] called as temperature cycling - cum - relaxation (TS) technique was used to evaluate both activation energy and activation area at a constant temperature and deformation structure. The details regarding the TASRA analysis is not presented here and are given elsewhere [17,58]. The reasons for anomalous behaviour of activation energy Q with temperature was examined in terms of possibilites, namely; the pre - exponential term $\dot{\epsilon}_o$ ($\dot{\epsilon} = \dot{\epsilon}_o exp(-\Delta G/kT)$) may or may not be constant, non-zero entropy of activation. The activation energy evaluated for both the cases of elastic and inelastic obstacles also showed a non - linear variation with temperature. In the temperature range (200 - 400 K) where the anamalous behaviour in activation energy with temperature was observed, the apparent activation area also showed a non - monotonic variation with σ or T. Fig. 6 shows the anomalous behaviour of activation energy (for either type of obstacle, with or without stress dependent pre - exponential factor) with temperature for Zr. The non - monotonic variation of activation area showing humps or plateaus is shown in Fig. 7. These anomalies in TASRA parameters have been attributed to DSA due to hydrogen in accordance with the findings of Reed-Hill and co-workers [59]. Thus DSA can be manifested as anomalies in the TASRA parameters.

For the sake of completeness, it is necessary to understand how DSA would effect TASRA results. It is now more or less established [2,60] that when DSA occurs there is an additional contribution from σ^*_f to the flow stress (Fig. 8a) from one or more of the sources, i.e. a contribution σ^*_{fd} from solute drag, a contribution $\sigma^*_{f\mu}$ from the increased work hardening due to greater dislocation multiplication and a contribution σ^*_f due to the reduction in ρ_m. For a given $\dot{\epsilon}$ the σ^*_f manifests itself only in a limited temperature range (between T_1 and T_2) and is maximum at T_p at which the velocities of strain ageing solutes and dislocations match, and this temperature T_p gets shifted to higher temperatures at high strain rates. Fig. 8b illustrates how DSA alters the $\sigma - \dot{\epsilon}$ variation and the contribution from σ^*_{fd} alone is considered assuming the constancy of structure and ρ_m. For very strong interactions giving rise to large σ^*_{fd}, σ becomes a multivalued function of $\dot{\epsilon}_p$ leading to a negative SRS and serrrated flow. A mild interaction on the other hand can result in a linear variation in log $\dot{\epsilon}_p$ Vs. σ plots in a temperature range leading to a constant value of apparent activation area and contributes to the anomalies in the activation energy variation. This was indeed the case for the results on Zr in the temerature ranging from 196 to 350 K. In this context it should be mentioned that the negative SRS is only a necessary condition for the onset of serrated flow but not the sufficient condition [28]. Further it is interesting to note that the analysis of flow transients during upward and downward jump in a titanium modified austenitic stainless steel at 300 K [61] indicated a slightly decreasing trend in the variation of steady state SRS with strain during a downward jump due to DSA, though no serrated flow was observed.

2.6 Grain Size Effect on DSA

The results of grain size effect on serrated flow [5-10] have shown that the ϵ_c required for the onset of serrated flow increases with increasing grain size. However Borchers etal. [62] and McCormick [63] found ϵ_c to be independent of grain size. Further it has been reported that the grain size significantly effects the other characteristics; i.e. the amplitude $\Delta\sigma_s$ of serration and the strain as well as the period between sucessive serrations. The amplitude of serrations [6, 8,18] and the strain period between sucessive serrations [7,9] have been found to decrease with increase in grain size. McCormick in an Al-Mg-Si alloy reported that the periodic locking serrations were observed only for grain sizes less than or equal to 0.14 mm and specimens with large grain size exhibited irregular serrated yielding. Further the strain ϵ_s between the sucessive serrations was found to be function of grain size d; $\epsilon_s \propto d^{-z}$ where Z = 0.2 independent of strain. Increasing grain size was found to decrease the value of $\Delta\sigma_s$.

Charnock model

Charnock [8] developed a theory to account for the grain size dependence of ϵ_c. He suggested that when the grain size dependence of dislocation density is considered in the vacancy model of DSA, the ϵ_c should depend on grain size at constant strain rate as; $\epsilon_c \propto d^{p}$,where $p = \frac{n'}{(m+\beta)}$. The value of n' can be evaluated from the grain size dependence of dislocation density. He demonstrated the agreement between theory and the experiment for α -brass. The critical strain equations as

discussed earlier in section 2.2.1 cane be written in a generalized form as

$$\rho_m(\epsilon)\, C_v(\epsilon) = K' \dot{\epsilon} \exp\left(Q_m/kT\right). \qquad \ldots\ldots(16)$$

It has been well established that at a constant strain, fine grained materials exhibit a higher dislocation density and Conrad and Christ [64] neglecting the low dislocation density present before deformation suggested that the dislocation density after deformation varies as

$$\rho_m = \frac{N \epsilon^{\beta}}{d^{n'}} \qquad \ldots\ldots(17)$$

where n' is dependent on ϵ . Charnock assumed the constancy of n' as in his study the strains were below 0.1. Incorporating this grain size dependence of dislocation density, the equation for ϵ_c can be expressed as

$$\epsilon_c = K_3\, d^{p}\, \dot{\epsilon}^{q} \exp\left[\frac{Q_m}{kT(m+\beta)}\right] \qquad \ldots\ldots(18)$$

where K_3 is a constant, $p = \frac{n'}{(m+\beta)}$ and $q = \frac{1}{(m+\beta)}$. The results of Charnock are in agreement with equation (18). However, other studies [5,7,9] have shown that the activation energy Q_m measured from the temperature dependence of ϵ_c is dependent on grain size. Charnock [65] has rationalised the dependence of Q_m with grain size through the dependence of n' on ϵ_c and has pointed out that reliable value of Q_m are those derived from experiments in which ϵ_c involved are very small,

i.e. less than 0.1. Charnock [8] suggested that the grain size dependence of ϵ_c arises from the influence of grain size on the average velocity of mobile dislocations. This, he arrives at from a simple logic. Equation (18) suggests that no serrated flow should be observed for single crystals. But experiments show that serrated flow is indeed observed in single crystals of α - brass [66]. It is important to note that in case of single crystals, even when oriented for multiple slip, the dislocation velocity will tend to be higher and the rate of dislocation interaction and hence the point defect production would be lower. Then the observed grain size dependence might be the result of either an increase in the average dislocation velocity of mobile dislocations or a decrease in the rate of production of point defects. The production of point defects would not be expected to depend on grain size, since it should be proportional to the number of dislocation interactions [37,67], and could be the result of few dislocations moving large distance in a coarse grained material or many dislocations moving short distance in a fine grained material. Further the contribution of point defect concentration was not taken into account by Charnock (cf. equation 18). In the Charnock model the grain size dependence arises from a dislocation velocity effect i.e. through the dislocation dependence of dislocation density.

2.7 Hall - Petch Relation and DSA

Numerous investigations have shown that the polycrystal flow stress σ_ϵ at given ϵ can be related to the average grain diameter d by the well known Hall - Petch relation [68,69]

$$\sigma_\epsilon = \sigma_{o\epsilon} + K_\epsilon d^{-1/2} \qquad \ldots\ldots(19)$$

where $\sigma_{o\epsilon}$ and K_ϵ are the experimentally determined constants known as Hall - Petch intercept and slope respectively. Many models have been proposed to explain the grain boundary strengthening effect and to account for the strain dependence of $\sigma_{o\epsilon}$ and K_ϵ. These have been reviewed by Li and Chou [70] and Johnston and Feltner [71]. Till date, there are mainly two models to explain the grain boundary strengthening effect, i.e. the dislocation pile up model [72-76] and the work-hardening model [70,77-79]. In the former model, the strengthening effect is described in terms of the stress concentration for the propagation of plastic deformation through grain boundary which is caused by dislocation pile up against the grain boundary and the propagation of deformation takes place by mechanisms such as:

i) the opearation of dislocation sources or generation of dislocations in the neighbouring grains,

ii) the passage of the leading dislocation of a pile up across the grain boundary,

iii) the emission of dislocations from ledges in a grain boundary.

Any of these effects on σ_ϵ enters as $d^{-1/2}$ in the Hall - Petch equation. The work hardening model is based on the fact that at a given strain, a high density of dislocations are accumulated inside the grains as grain size decreases. The difference between the two models arises from the ideas that the controlling factor for plastic deformation is the stress for the generation and multiplication or that for the movement of dislocations. The higher density of dislocation accumulation with decreasing grain size leading to higher flow stresses for fine grained materials can be rationalised according to

(a) the geometrically necessay dislocations are introduced to

accommodate the incompatibility of deformation between the grains,

(b) the shortening of slip distance in finer grain materials requires the increase in dislocation density to give a certain strain compared with coarse grained materials.

Till date there is no theory to predict uniquely the strain dependence of Hall - Petch constants. In a recent study Sangal etal. [80] suggested the role of extrinsic grain boundary dislocations in explaining the strain dependence of Hall - Petch constants. Further it has been suggested by Narutami etal. [81] that dislocation multiplication due to the interaction between the geometrically necessary dislocations and the primary dislocations inside the grains have to be considered.

There have been few studies on the grain size effect on tensile behaviour in type 316 stainless steel [82,83]. A high value of K_ϵ found in type 316 stainless steel [82] has been attributed to the segregation of alloying elements to grain boundaries. It has been mentioned earlier that in the DSA regime K_ϵ would show a peak with temperature. Kutumba Rao etal. [84] in their studies on a Cr-Mn-N austenitic stainless steel observed that $\sigma_{0.6}$ was found to decrease monotonically with increase in temperature upto 873 K, while K_ϵ exhibited a peak in the temperature range from 575 to 775 K and decreasing with temperature on either side of this temperature range. According to Armstrong [85,86], this peak in K_ϵ with temperature is interpreted as due to DSA in grain boundary regions.

3. RESULTS OF GRAIN SIZE EFFECT ON DSA (Mannan, 1981)

It has been mentioned earlier that the serrations represent only one of the manifestaions of DSA and various other anomalies due to DSA have been introduced (cf. section 2.4). In this section, the results of

effect of grain size on various aspects of DSA for a type 316 stainless steel are discussed with a view to elucidating the role of grain boundaries in DSA. The effect of grain size on flow and work hardening behaviour have been presented before discussing the analysis of Hall - Petch constants in DSA regime and the influence of grain size on serrated yielding. The details of the treatments given to produce various grain sizes and of the test methods employed are described elsewhere [16,87].

3.1 Effect of Grain size on the Flow stress and Work Hardening

The effect of grain size on the deformation bahaviour of type 316 austenitic stainless steel has been described in detail elsewhere [16,88] and the results discussed here pertain only to grain size effects on DSA. Fig. 9 shows the variation with temperature of 0.2% yield stress normalised with Young's modulus E for different grain sizes. The yield stress decreases with temperature to about 523 K, beyond which a well defined plateau is observed in the temperature range $\sim$ 523 - 923 K, followed by rapid fall again at higher temperatures. Further a general tendency for the plateau region to extend to higher temperatures with increase in grain size is observed. A similar behaviour for the variation of flow stresses at higher strains and of ultimate tensile strength with temperature was observed except that the plateau changed over to a pronounced hump at higher strains [16]. As has been already mentioned and it is now more or less well established [12,15,84,89,90] that plateaus/humps in the variation of flow stress with temperature result from DSA. A plot of average work hardening rate normalised with respect to temperature dependence of elastic modulus, θ/E (where $\theta = \frac{\sigma_{0.05} - \sigma_{0.005}}{0.045}$) as a function of

temperature is shown in Fig. 10 for the different grain sizes. It is clear from the figure that the work hardening rate increases with temperaure, shows a peak around 923 K and then decreases at higher temperatures and this behaviour is in agreement with earlier studies [89,90]. It is important to note that the fine grained material shows a higher work hardening rate when compared with coarse grained material. Further, the flow stress plateaus and peaks as well as increase in the average work hardening rate occur over the same temperature and grain size range in which serrated yielding was observed and the results on serrated flow are covered in the later part of this section. The two important observations in the DSA region are the increase of flow stress and work hardening rate; the former effect arises due to larger dislocation density at a given strain compared with that at other temperatures and the latter effect can also be correlated with the more rapid increase in dislocation density. Further the higher work hardening rate observed in fine grained material as compared with coarse grained material could result from the higher rate of increase in dislocation density in fine grained material. It is observed that the work hardening peak occurs towards the upper end of DSA temperature range. This observation is consistant with the fact that this temperature range represents conditions for strong pinning and accordingly the temperature of most rapid and strongest dislocation immobilization, leading to an increased rate of dislocation accumulation [3]. Similar results have been reported by Kim and Hall [91] in α-brass. The observed decline in work hardening above $\sim$ 923 K has been attributed to the precipitation of carbides [89] depleting the matrix of solutes responsible for dislocation locking as well as to dynamic recovery [90].

3.2 Hall - Petch Analysis in DSA Regime

In this section the temperature dependence of Hall - Petch constants and in particular the humps in the variation of Hall - Petch slope with temperature which also manifests as plateaus or humps in the flow stress - temperature and work hardening - temperature variations are discussed. As mentioned earlier the value of K_ϵ found in type 316 stainless steel is higher than that observed for other fcc metals (cf. section 2.7). The variation of $\sigma_{o\epsilon}$ and K_ϵ with temperature is shown in Figs. 11 and 12 respectively. It is normal to expect that both $\sigma_{o\epsilon}$ and K_ϵ to decrease with increase in temperature (Fig. 11), but at higher temperaures between 523 and 723 K, K_ϵ shows an increase thus resulting in the occurrence of a peak in K_ϵ Vs. temperature curves. Such a peak in the variation of K_ϵ with T is one of the manifestations of DSA as mentioned earlier. On the other hand $\sigma_{o\epsilon}$ shows a smooth decrease with increase in temperature (Fig. 12). Similar results have been reported in a Cr-Mn-N austenitic stainless steel [84]. Armstrong [85] demonstrated that $\sigma_{o\epsilon}$ reflects deformation processes in the grain interiors, while K_ϵ reflects those in the grain boundary regions. Thus the monotonic decrease of $\sigma_{o\epsilon}$ with T may be attributed to decreasing lattice fricition. Similarly if the general tendency for K_ϵ to decrease with increasing temperature is interpreted as weakening of the locking effects at grain boundaries, then the increase in K_ϵ between 523 K and 723 K may be attributed to a mechanism which contributes to additional locking at grain boundaries in this temperature range. This additional locking could occur as a result of DSA in grain boundary regions [16,84,86,92,93]. Further the fact that the flow stress and work hardening peaks become more pronounced at finer grain size is a further reason for concluding that grain boundary regions are the preferred

sites for DSA.

In summary, owing to the DSA at intermediate temperatures (523 - 923 K) through additional locking of dislocations in the grain boundary regions, humps in the Hall - Petch slope variation with temperature results, which also manifests as plateaus or humps in the flow stress - temperature and work hardening - temperature variations. The important conclusion is that the grain boundary regions are the preferred sites for DSA. The other manifestations of DSA, i.e. serrated flow and grain size effect on various characteristics of serrtaed flow are presented below.

3.3 Grain Size Effect on Serrated Yielding

In this section the resluts on the effect of grain size on the nature of serrations and critical strain for the onset of serrated flow are presented and the detailed account of DSA is given elsewhere [87]. Typical load - elongation curves illustrating the effect of temperature on the nature of serrated flow for various grain sizes are shown in Figs. 13 to 17. No serrations were observed at temperatures less than 523 K. From about 523 to 723 K irregular but consistant instabilities were detected. Type A serrations were found to occur around 823 K and changed over to type B at higher strains and at higher temperatures (Fig. 13). The grain size showed a marked influence on the nature of serrations. Periodic type A locking serrations observed in fine grained material (Fig. 13) changed over to irregular serrations in coarse grained material (Fig. 17). Unlocking type C serrations were observed only for coarse grain sizes at higher temperatures (Fig. 15). Serrated flow was found to occur for fine grained material upto 873 K while it persisted upto 973 K for coarse grain sizes. The lowest temperature at

which instabilities in flow curves were recorded in fine grain size material was 523 K (Fig. 13) while these were noticed for coarse grain sizes only at and above 623 K (Figs. 16 and 17). For type A serrations, the amplitude of stress drop $\Delta\sigma_s$ for each serration and the strain between sucessive serrations ϵ_s were found to increase with increase in plastic strain and there was a tendency for $\Delta\sigma_s$ and ϵ_s to decrease with increase in grain size. The results of influence of grain size on the nature of serrations, i.e. the periodic type A serrations observed for fine grain sizes and coarse grain sizes exhibiting irregular serrations are in agreement with the results reported by McCormick [63]. The decrease in $\Delta\sigma_s$ with increase in grain size is in accordance with earlier investigators [6,8,18]. In conventional yielding, the yield drop [2,94] and the Lüders strain [95,96] decreases with increase in grain size. If each serration in PLE is the result of a localised yield point corresponding to the serration amplitude and a Luders strain corresponds to a serration period, the observed grain size effect would be expected if the distance through which the band propagates is approximately the same for each grain size [8].

Fig. 18 shows that the log - log plots of critical strain against grain size at temperatures of 823 K and 873 K are stright lines with a slope $\simeq$ 0.6. This corresponds to the value of p = 0.6 in the grain size dependence of ϵ_c in equation (18). This value compares favourably with the values of p (i.e. 0.5 to 0.75) reported by others [8,9]. The studies on Al-Mg [5,6] and Cu-Sn [10] alloys have shown that ϵ_c increases with increase in grain size. On the other hand, McCormick [63] and Borchers etal. [62] found ϵ_c to be independent of grain size. It is already mentioned (equation 18) that the value of p can be found if n' and $(m+\beta')$ are known, where n' is the exponent for the grain size

dependence of dislocation density and $(m+\beta)$ is the term due to strain dependence of ρ_m and C_v. The value of n' was not determined experimentally, but it can be assumed to be close to unity from the available experimental results [8,97]. Then the value of $(m+\beta)$ is necessary to estimate the value of p assuming $n' = 1$. Fig. 19 shows the variation of ϵ_c with $\dot{\epsilon}$ for two grain sizes (0.06 and 0.270 mm) at different temperatures in the range from 723 to 873 K. The determined value of $(m+\beta)$ equal to 2.3 is found to be independent of temperature and grain size. Thus knowing $(m+\beta)$ equal to 2.3, p can be obtained as p $\simeq$ 0.43 which compares well with experimentally determined value of 0.60. This agreement suggests the validity of Charnock's model [8] and the influence of grain size arises predominantly from a dislocation density effect since no grain size dependence of point defect concentration is taken into account in Charnock's model.

Fig. 20 shows the plots of log ϵ_c against 1/T for the two grain sizes of 0.060mm and 0.270 mm and the values of apparent activation energy was found to be $\simeq$ 255 kJ/mol and is independent of grain size. This is compatible with the contention that the diffusion of substitutional solutes i.e. Chromium may be responsible for DSA [87].

3.4 Effect of Thermal Ageing on Serrated Flow

The serrated yielding behaviour in a type 316 stainless steel has been studied in the temperature range from 300 to 923 K and two regimes of serrated flow have been reported [98]; the low temperture regime (523 - 623 K) with $(m+\beta) = 2.3$ and $Q_m = 138$ kJ/mol was attributed to the diffusion of interstitial solutes to dislocations, while the substitutional solutes like Cr were considered responsible for serrated flow in the high temperature regime (673 - 923 K). The values of $(m+\beta)$

and Q_m were found to be 2.3 and 277 kJ/mol in the high temperature region. The effect of prior ageing in the temperature range (823 - 1323 K) for different periods of time, on the serrated yielding behaviour at 923 K is presented in this section. Serrated flow completely disappeared from the flow curve at 923 K (at $\dot{\epsilon} = 3 \times 10^{-4}$ s^{-1}) after certain time - temperature combination of ageing as shown in Fig. 21. Ageing has been shown to influence serrated flow and it has been reported in Mg-Al alloy [99], Al-Mg-Si alloy [100] and 6063 alloy [101] that certain time - temperature combinations can casue disapperance of serrations. Further, neutron irradiation [102] has been found to supress DSA which was otherwsie observed in an unirradiated mild steel at 473 K.

As mentioned earlier in section 2.3, Hayes and Hayes [56] have proposed two possible ways by which serrations disappear from the flow curve at high temperatures namely a critical strain delay mechanism (carbon diffusing down the dislocation line to a precipitate sink) or by a progressively smaller strain to the disppearance of serrations off the end of the flow curve (carbon reacting with a carbide - forming species on the dislocation line). The mechanism leading to the disappearance of serrated flow is a reaction occurring between the carbide forming substitutional atoms and carbon atmospheres which are forming on the arrested dislocations. This leads to the depletion of carbon atmospheres and the serrated flow disappeares when the net carbon on the dislocation decreases to a value below the critical concentration. The rate controlling process for the disapperance of serrations is the rate of diffusion of substitutional carbide forming species to the arrested dislocation line. Hayes and Hayes [56] have shown that the disappearance of the serrated flow in 2.25 Cr - 1 Mo is related to the distribution of

carbides and the composition of carbide sinks and both of these are dependent on the tempering temperatures employed.

In type 316 stainless steel, the first phase to form due to ageing is $M_{23}C_6$ type carbide followed by other intermetallics like laves, chi and sigma phases. $M_{23}C_6$ precipitates sucessively on grain boundaries, incoherent twin boundaries, coherent twin boundaries and finally intragranularly. The grain boundary regions which have a higher concentration of solute atoms compared to that in the matrix can serve as preferential sites for DSA and grain boundary precipitation thus should influence the serrated yielding behaviour. The results as shown in Fig. 21 can be explained as follows. Disappearance of serrations can occur by a strain delay mechanism particularly when precipitate sinks are present. With increasing density of carbide precipitates which act as sinks for drainage of carbon from dislocations, the critical concentration of carbon around dislocations required for serrated flow might not build up and this would result in a smooth stress-strain curve. Ageing for longer durations lead to coarsening of the precipitates, reducing the precipitate density at grain boundaries and thereby weakening the effect of precipitate sinks to drain off carbon. This will reintroduce serrated flow. Similarly ageing at higher temperatures or ageing at lower temperature for a longer duration can redissolve the precipitates and serrations can appear on the flow curve. Thus the role of precipitates at the grain boundary on the disappearance of serrated flow further supports the role of grain boundaries as preferred sites for DSA in austenitic stainless steels.

3.5 Effect of Grain Size On DSA During LCF

The details regarding the effect of grain size on LCF properties and the role of grain size on DSA in LCF properties for a type 304 stainless steel have been discussed elsewhere [103 - 105]. Only a brief summary on the influence of grain size on DSA during LCF behaviour in an AISI type 304 stainless steel is presented in this section. Three grain sizes were studied namely 75, 310 and 700 μm. DSA manifests during cyclic deformation in the form serrations in stress - strain hysteresis loop and various other manifestations that are commonly observed. include:

i) Large normalised cyclic hardening ($(\Delta\sigma/2)_{max}/(\Delta\sigma/2)_1$), where $(\Delta\sigma/2)_1$ is the first cycle tensile stress amplitude and $(\Delta\sigma/2)_{max}$ is the maximum tensile stress amplitude and the ratio increases with decreasing $\dot{\epsilon}$,

ii) an increase in the number of cycles to attain $(\Delta\sigma/2)_{max}$ with decreasing $\dot{\epsilon}$,

iii) for a given total strain range, plastic strain range decreases with increasing temperature or decreasing $\dot{\epsilon}$,

iv) increase in stress response with decreasing $\dot{\epsilon}$ (negative SRS) or increasing temperature.

The exploratory tests [103] revealed DSA peak temperature to be around 823 K. Grain size was found to have influence on the type of serrations. Generally irregular or mixed type A and type B serrations were observed in all the grain sizes, but at the lowest frequency (0.001 HZ) and at 923 K unlocking serrations were observed.

Table 1 summarises the influence of grain size on LCF properties at different strain rates. Broadly, the grain size effect can be summarised as; number of cycles to failure N_f decreases markedly with

decreasing $\dot{\epsilon}$ for all grain sizes and a minimum in N_f is observed for medium grain size material at the two lower strain rates. The observerd loss of N_f with decreasing $\dot{\epsilon}$ for all grain sizes arises due to DSA as evidenced by the increase in maximum stress amplitude and a decrease in plastic strain range with decreasing $\dot{\epsilon}$. It needs to be emphasised that DSA enhances the inhomogenity of deformation during LCF due to solute locking of slow moving dislocations between the slip bands. This in turn leads to pronounced planar slip to occur and the impingement of these slip bands on grain boundaries causes intergranular brittle decohesion and consequent reduction in life. TEM observations revealed that dislocation substructure was dependent on grain size and strain rate. The substructure, in fine grain size at all strain rates and at higher strain rate (1.6×10^{-2} s^{-1}) for medium and coarse grain sizes, was characterised by randomly distributed dislocations. Whereas, well developed planar slip bands were observed in medium and coarse grain sizes at lower strain rates. The degree of intergranular cracking was more in medium grain size which led to pronounced decrease in N_f.

4. GRAIN SIZE EFFECTS ON DSA IN Zr (Rodriguez, 1976)

The observed anomalies in the various TASRA parameters for Zr in the temperature range from 200 - 400 K have been explained based on DSA due to hydrogen (cf. section 2.5). It is important to mention that in the studies on Zr (with 0.055 mm grain diameter) around 300 K, an inflexion in the variation of work - hardening rate with temperature was observed, while a plateau in the total elongation and a mild minimum in uniform elongation was noticed. These are the indications of manifestation of DSA. In this section some interesting analysis of Hall - Petch constants in the DSA temperature range is discussed. The various

grain sizes studied ranged from 0.032 mm to 0.116 mm and the details regarding the heat treatments and test methods have been given elsewhere [17]. The Hall - Petch relation was found to be valid at all temperatures (77 - 543 K); both $\sigma_{0\epsilon}$ and K_ϵ varied with strain and temperature. The intercept $\sigma_{0\epsilon}$ increased with increasing strain and decreased with increasing temperature. While K_ϵ was generally found to decrease with temperature and to increase with strain except at higher temperatures (483 and 543 K) where K_ϵ decreased with strain at higher strains. The dependence of $\sigma_{0\epsilon}$ and K_ϵ on strain were analysed by Rodriguez [17] according to various theories of grain boundary strengthening. In the temperature region between 196 and $\sim$ 400 K, the linear increase of K_ϵ with $\epsilon_p^{1/2}$ showed that the interpretation based on dislocation density models ($K_\epsilon = \beta \mu b B^{1/2} \epsilon_p^{1/2}$) or based on modification by Takeuchi [106] ($K_\epsilon = c' \beta \mu b B^{1/2} \epsilon_p^{1/2}$, where β is the strengthening efficiency of dislocations and C' chracterizes the decrease of hardening with formation of cell structure) also could not explain the linear increase of K_ϵ and this unexpected behaviour arises due to DSA. The observed variation of $\sigma_{0\epsilon}$ and K_ϵ with strain was in conformity with Ashby's concept of polycrystal workhardening arising from geometrically necessary dislocations (dependent on grain size) and statistically stored dislocations (independent of grain size). Further it is important to mention the result from temperature cycling experiments that the thermal component of the flow stress is contained wholly in $\sigma_{0\epsilon}$ and is independent of grain size [17] unlike the results on soft hcp metal like Cd where it was contained in the $K_\epsilon d^{-1/2}$ term [107].

The influence of DSA on the Hall - Petch parameters is clearly illustrated in Fig. 22 in which K_ϵ, K_ϵ / μ and $\sigma_{0\epsilon}$ are plotted against temperature. The humps and non - monotonic variations in these plots

occur in the same temperature range where the various other anomalies due to DSA are found. It has been pointed out that the peak in the variation of K_ϵ with T is one of the manifestations of DSA (cf. sections 2.4, 2.7 and 3.2). It is interesting to note from Fig. 22(a) and (c) the difference in the effect of strain on the strain ageing hump in K_ϵ and $\sigma_{o\epsilon}$. At higher strains, the hump in K_ϵ is more pronounced while the hump in $\sigma_{o\epsilon}$ seems to be less pronounced (Fig. 22(a) and (c)). This would imply that the strain ageing contribution to K_ϵ is mainly through $\sigma^*_{f\mu}$ whereas it is σ^*_f and/or σ^*_{fd} that are mainly contributing to $\sigma_{o\epsilon}$ (cf. section 2.5). Another interesting observation is the fact that K_ϵ/μ (K_ϵ normalised with temperature dependence of modulus μ, with $\mu = C_{66}$) at vary low strains (0.002) is almost temperature independent, while at higher strains, in addition to the strain ageing peak, a greater and definite temperature dependence for K_ϵ/μ is seen (Fig. 22(b)) which is due to the variation of β or C' (where β and C' are the parameters in $K_\epsilon - \epsilon_p$ relation). Thus at low strains the variation of K_ϵ with temperature is proportional to the shear modulus, while at higher strains, it is more than predicted by the shear modulus. To conclude, the results indicate the manifestation of DSA for Zr in the temperaure range from 200 to 400 K.

5. SUMMARY

The various aspects of DSA, models for serrated flow from DSA, anomalies in TASRA parameters due to DSA and the results of grain size effects on DSA emphasising the role of grain boundaries in DSA along with some interesting analysis of Hall - Petch equation in the DSA regime have been clearly brought out in this report. The plateus or humps exhibited in the variation of flow stress and work hardening with temperature in conjunction with humps in the variation of Hall - Petch slope with temperature, all reveal that the DSA effects are pronounced for fine grain size materials. The important conclusion that stems from these observations is that the grain boundary regions are preferred sites for DSA. Further this conclusion is also arrived at from the studies pertaining to effect of thermal ageing on serrated flow. Mainly, there are two important conclusions drawn from the analysis of grain size effect on the critical strain for the onset of serrated flow, i.e. the critical strain increases with increase in grain size and this dependence arises due to grain size dependence of dislocation density. Finally it needs to be emphasised that both factors,i.e. the incidence of larger dislocation density and the rate of increase in dislocation density in DSA regime become more pronounced for fine grain sizes compared to coarse grain size materials.

ACKNOWLEDGEMENTS

I greatfully acknowledge the collaboration of Mr C. Phaniraj and Dr S.L. Mannan in the preparation of this lecture. Thanks are also due to Mr M. Nandagopal, Mrs R. Umamaheswari, Mr P.C. Gopi and Mr S. Sakthy for their valuable help.

REFERENCES

1. A. Portevin and F. Le - Chatlier, C.r. Acad. Sci. 176, 507(1923).

2. B.J. Brindley and P.J. Worthington, Metals Mater. 4, 101(1970).

3. R.E. Reed-Hill, Rev. High Temp. Mater. 2, 214(1974).

4. P. Rodriguez, Bull. Mater. Sci. 6, 653(1984); see also P. Rodriguez, in R.W. Cahn (ed.), Encyclopedia of Mater. Sci. Engng. - Supplementary, Vol. 1, Pergamaon, pp. 504-508 (1988).

5. B.J. Brindley and P.J. Worthington, Acta. metall. 17, 1357(1969).

6. S. Miura and H. Yamaguchi, Trans. Japan Inst. of Metals 13, 82(1972).

7. D. Munz and E. Macherauch, Z. Metall Kd. 57, 552(1966).

8. W. Charnock, Phil. Mag. 18, 89(1968).

9. O. Vohringer and E. Macherauch, Z. Metall Kd. 58, 317(1967).

10. D.J. Lloyd and P.J. Worthington, Phil. Mag. 24, 195(1971).

11. J.T. Barnby, J. Iron and Steel Inst. 204, 23(1966).

12. C.F. Jenkins and G.V. Smith, Trans. metall. Soc. A.I.M.E. 245, 2149(1969).

13. R. Tamahankar, J. Plateau and C. Crussard, Rev. Metall. 55, 383(1958).

14. R.D. Naybour, Acta. metall. 13, 1197(1965).

15. L.H. De Almeida, I. Le May and S.N. Monteiro, Proc. Second. Int. Conf. on Mechanical Behaviour of Materials, Am. Soc. Metals, Metals Park, p.1697(1976)

16. S.L. Mannan, Ph. D thesis, Indian Inst. Sci., Bangalore(1981).

17. P. Rodriguez, Ph. D thesis, Indian Inst. Sci., Bangalore(1976).

18. B. Russel, Phil. Mag. 8, 615(1963).

19. A.J.R. Solar - Gomej and W.J. McG. Tegart, Phil. Mag. 20, 495(1969).

20. E. Pink and A. Grinberg, Mater. Sci. Engng. 51, 1(1981).

21. A. Wijler, J. Schade Van Westrum and A. Van den Beukel, Acta. metall. 20, 355(1972).

22. S. Venkadesan, Ph. D thesis, Indian Inst. Technol., Madras(1991).

23. S. Venkadesan, C. Phaniraj, P.V. Sivaprasad and P. Rodriguez, Acta. metall. 40, 569(1992).

24. S. Venkadesan, P.V. Sivaprasad, C. Phaniraj and P. Rodriguez, Z. MetallKd. 84, 206(1993).

25. S. Venkadesan, S. Venugopal, P.V. Sivaprasad, and P. Rodriguez, Mater. Trans. J.I.M. 33, 1040(1992).

26. A.H. Cottrell, Phil. Mag. 74, 829(1953).

27. P.G. McCormick, Acta. metall. 20, 351(1972).

28. A. Van den Beukel, Physica Status Solidi(a) 30, 197(1975).

29. R.A. Mulford and U.F. Kocks, Acta. metall. 27,1125(1979).

30. A.W. Sleeswyk, Acta. metall. 6, 598(1958).

31. W.S. Gorsky, Phys. Z. Sowjet. 8, 457(1935).

32. A.H. Cottrell, Report on Strength of Solids, Phys. Soc. London, p.30(1948).

33. A.H. Cottrell and B.A. Bilby, Proc. Phys. Soc. A 62, 49(1949).

34. A.H. Cottrell and M.A. Jawson, Proc. Royal Soc. A 199, 104(1949).

35. J.P. Hirth and J. Lothe, Theory of Crystal Dislocations, New York, Mc Graw - Hill(1968).

36. F. Seitz, Adv. Phys. 1, 43(1952).

37. H.G. Van Bueren, Imperfections in Crystals, North - Holland, Amsterdam(1961).

38. R.K. Ham and D. Jaffrey, Phil. Mag. 15, 247(1967).

39. R.E. Reed-Hill and Tuling Zhu, High Temp. Mater. Processes 6, 93(1984).

40. A. Van den Beukel, Acta metall. 28, 965(1980).

41. P. Penning, Acta. metall. 20, 1169(1972).

42. A. Wijler and J. Schade Van Westrum, Scripta metall. 5, 159(1971).

43. A. Van den Beukel and U.F. Kocks, Acta metall. 30, 1027(1982).

44. L.P. Kubin and Y. Estrin, Acta metall. 38, 697(1990).

45. A. Korbel, J. Zasadzinski and Z. Sieklucka, Acta. metall. 24, 919(1976).

46. S. Radelaar, D.J. Lloyd and P.J. Worthington, Scripta metall. 4, 743(1970).

47. K.L. Neelakantan and G. Venkataraman, Acta metall. 31, 77(1983).

48. G. Ananthakrishna, Bull. Mater. Sci. 6, 665(1984).

49. J.L. Strudel, in Deformation - All Aspects, Inter. Conf. on metal Sci., ICMS, Ranchi, Indian Inst. Metals(1983).

50. S.L. Mannan and P. Rodriguez, Phil. Mag. 25, 673(1972).

51. J. Weertman, Can. J. Phys. 45, 797(1967).

52. S.R. Bodner and A. Rosen, J. Mech. Phys. Solids 15, 63(1967).

53. A. Rosen and S.R. Bodner, Mater. Sci. Engng. 4, 115(1969).

54. W. Charnock, Phil. Mag. 20, 427(1969).

55. R.W. Hayes, Acta. metall. 31, 365(1983).

56. R.W. Hayes and W.C. Hayes, Acta. metall. 32, 259(1984).

57. P. Rodriguez, Trans. Indian Inst. Metals 31, 371(1978).

58. P. Rodriguez and S.K. Ray, Bull. Mater. Sci. 10, 133(1988).

59. A.T. Santhanam and R.E. Reed-Hill, Met. Trans. 2, 2619(1971).

60. J.D. Baird, Met. Rev. 15, 1(1971).

61. S. Venkadesan, P. Rodriguez, K.A. Padmanabhan, P.V. Sivaprasad and C. Phaniraj, Mater. Sci. Engng. A154, 69(1992).

62. H. Borchers, H.M. Tensi and H. Ehrhardt, Z. MetallKd. 58, 863(1967).

63. P.G. McCormick, Phil. Mag. 23, 949(1971).

64. H. Conrad and B. Christ, Recovery and Recrystallisations of Metals, edited by L. Himmel (New York : Interscience), p.124(1963).

65. W. Charnock, Phil. Mag. 20, 209(1969).

66. G.W. Ardley and A.H. Cottrell, Proc. R. Soc. A219, 328(1953).

67. H.G. Van Bueren, Acta. metall. 3, 519(1955).

68. E.O. Hall, Proc. Phys. Soc. B64, 747(1951).

69. N.J. Petch, J. Iron Steel Inst. 174, 25(1953).

70. J.C.M. Li and Y.T. Chou, Metall. Trans. 1, 1145(1970).

71. T.L. Johnston and C.E. Feltner, Metall. Trans. 1, 1161(1970).

72. A.H. Cottrell, Trans. metall. Soc. A.I.M.E. 212, 192(1958).

73. R.W. Armstrong, I. Codd, R.M. Douthwaite and N.J. Petch, Phil. Mag. 7, 45(1962).

74. J.D. Meakin and N.J. Petch, Phil. Mag. 29, 1149(1974).

75. W.L. Philips and R.W. Armstrong, Metall. Trans. 3, 2571(1972).

76. A.H. Cottrell, Relation Between Structure and Strength in Metals and Alloys, p. 456, H.M.S.O., London(1963).

77. H. Conrad, Electron Microscopy and Strength of Crystals, edited by G. Thomas and J. Washburn, Interscience, New York, 1963, p.299.

78. A.W. Thompson and M.I. Baskes, Phil. Mag. 28, 301(1973).

79. M.F. Ashby, Phil. Mag. 21, 399(1970).

80. S. Sangal, K.J. Kurzydlowski and K. Tangri, Acta metall. 39, 1281(1991).

81. T. Narutami and J. Takamura, Acta metall. 39, 2037(1991)

82. J.A. Scott and J.E. Spruiell, Metall. Trans. 5, 255(1974).

83. L.A. Norstrom, Metal Sci. 11, 208(1977).

84. V. Kutumba Rao, D.M.R. Taplin and P. Rama Rao, Metall. Trans. 6A, 77(1975).

85. R.W. Armstrong, Acta. metall. 16, 347(1968).

86. R.W. Armstrong, in Dislocation Dynamics, edited by A.R. Rosenfield etal, Mc Graw Hill, New YorK, 1968, p.293.

87. S.L. Mannan, K.G. Samuel and P. Rodriguez, Trans. Indian Inst. Metals 36, 313(1983).

88. S.L. Mannan, K.G. Samuel and P. Rodriguez, Proc. 6-th Int. Conf. on Strength of Metals and Alloys, Melborne p. 637(1982).

89. J.T. Barnby, J. Iron. Steel Inst. 203, 392(1965).

90. D.J. Michel, J. Moteff and A.J. Lovell, Acta. metall. 21, 1269(1973).

91. I.S. Kim and E.O. Hall, Metals Forum 1, 95(1978).

92. R.W. Armstrong, J.H. Bechtold and R.T. Begley, in Refractory Metals and Alloys II, Vol. 17(Eds. M. Semchyshen and I. Perlmutter), Intersci., New York, p.159(1963).

93. D.J. Dingley and D. Mc Lean, Acta. metall. 15, 885(1967).

94. N.J. Petch, Acta. Metall. 12, 59(1964).

95. R.W. Evans, J. Iron. Steel Inst. 205, 1150(1967).

96. D. Mc Lean, Mechanical Properties of Metals (J.Wiley), 190(1962).

97. J.W. Edington and R.E. Smallman, Acta. metall. 12, 1913(1964).

98. K.G. Samuel, S.L. Mannan and P. Rodriguez, Acta. metall. 36, 2323(1988).

99. M. Chaturvedi, D.J. Lloyd and K. Tangri, Metals Sci. J. 6, 16(1972).

100. H.J. Harun and P.G. McCormick, Acta metall. 27, 155(1979).

101. D.M. Riley and P.G. McCormick, Acta metall. 25, 181(1977).

102. K. Lingamurthy, Scripta metall. 18, 87(1984).

103. K. Bhanu Sankara Rao, Ph. D Thesis, Univ. of Madras (1989).

104. K. Bhanu Sankara Rao, M. Valsan, R. Sandhya, S.L. Mannan and P. Rodriguez, Trans. Indian Inst. Metals 44, 255(1991).

105. S.L. Mannan (MRSI medal lecture) to appear in Bull. Mater. Sci. (1993).

106. T.Y. Takeuchi, J. Phys. Soc. Japan 28, 935(1972).

107. S.L. Mannan and P. Rodriguez, Acta metall. 23, 221(1975).

Table-1

Low cycle fatigue properties as a function of Grain Size and $\dot{\epsilon}$ at 823 K ($\Delta\epsilon_t$ = 0.80%)

Grain size (μm)	$\dot{\epsilon}$ (s^{-1})	$\Delta\epsilon_p$ (%)	$(\frac{\Delta\sigma}{2})_1$ (MPa)	$(\frac{\Delta\sigma}{2})_{max}$ (MPa)	N_1	N_p	N_f	Remarks
75	1.6×10^{-2}	0.569	183	238	900	169	1069	O
75	1.6×10^{-3}	0.480	159	271	800	490	1290	◒
75	1.6×10^{-4}	0.424	138	279	550	246	796	●
310	1.6×10^{-2}	0.567	159	227	600	1790	2390	O
310	1.6×10^{-3}	0.562	147	262	160	555	715	◒
310	1.6×10^{-4}	0.555	112	271	220	209	429	●
700	1.6×10^{-2}	0.500	113	232	550	2450	3000	O
700	1.6×10^{-3}	0.412	102	255	500	775	1275	◒
700	1.6×10^{-4}	0.368	108	278	450	375	875	●

O smooth stress-strain hysteresis loops, ◒ smooth stress-strain hysteresis loops + dynamic strain ageing.

● serrated flow in the plastic regions of stress-strain hysteresis loops.

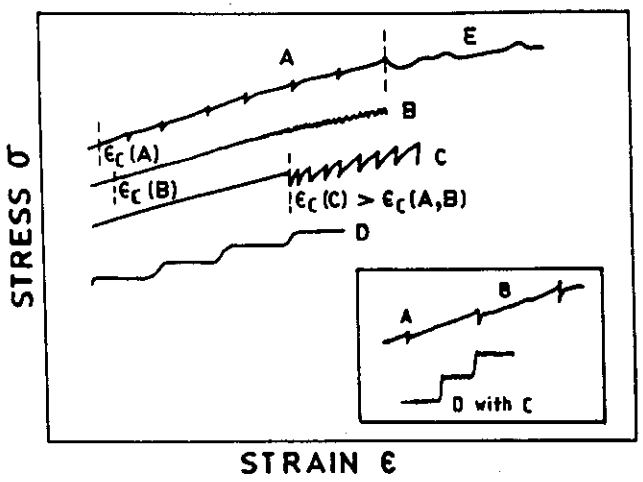

Fig. 1. Types of serrations [Ref. 4].

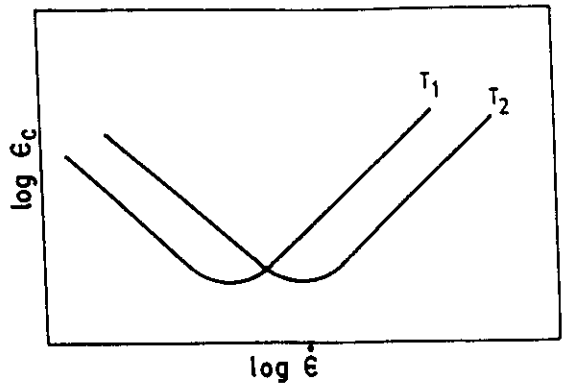

Fig. 2. Effect of strain rate and temperature on critical strain; $T_2 > T_1$ [Ref. 4].

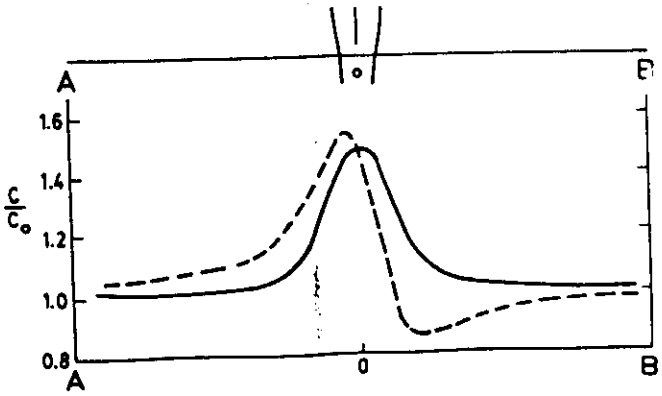

Fig. 3. Concentration of solute atoms along the line AOB near a dislocation; full line - stationary dislocation; broken line - dislocation moving slowly towards B [Ref. 34].

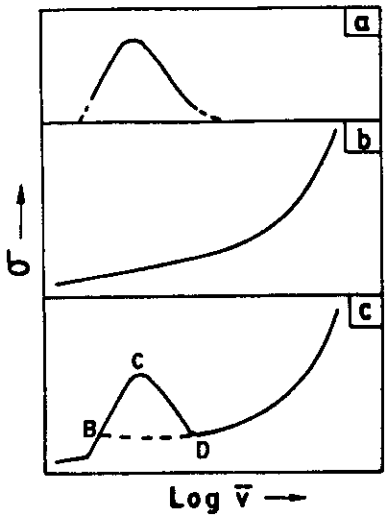

Fig. 4. (a) The solute drag stress on a dislocation as a function of dislocation velocity. (b) Normal stress-velocity relation for dislocation in the absence of the drag stress. (c) Actual stress - velocity variation due to the presence of a drag stress at intermediate velocities [Ref. 4,35].

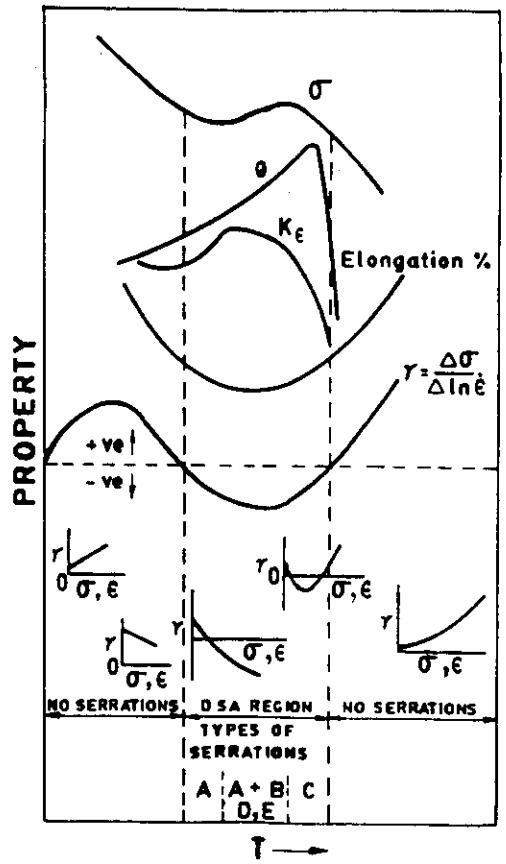

Fig. 5. Schematic illustration of the various manifestations of dynamic strain ageing [Ref. 4].

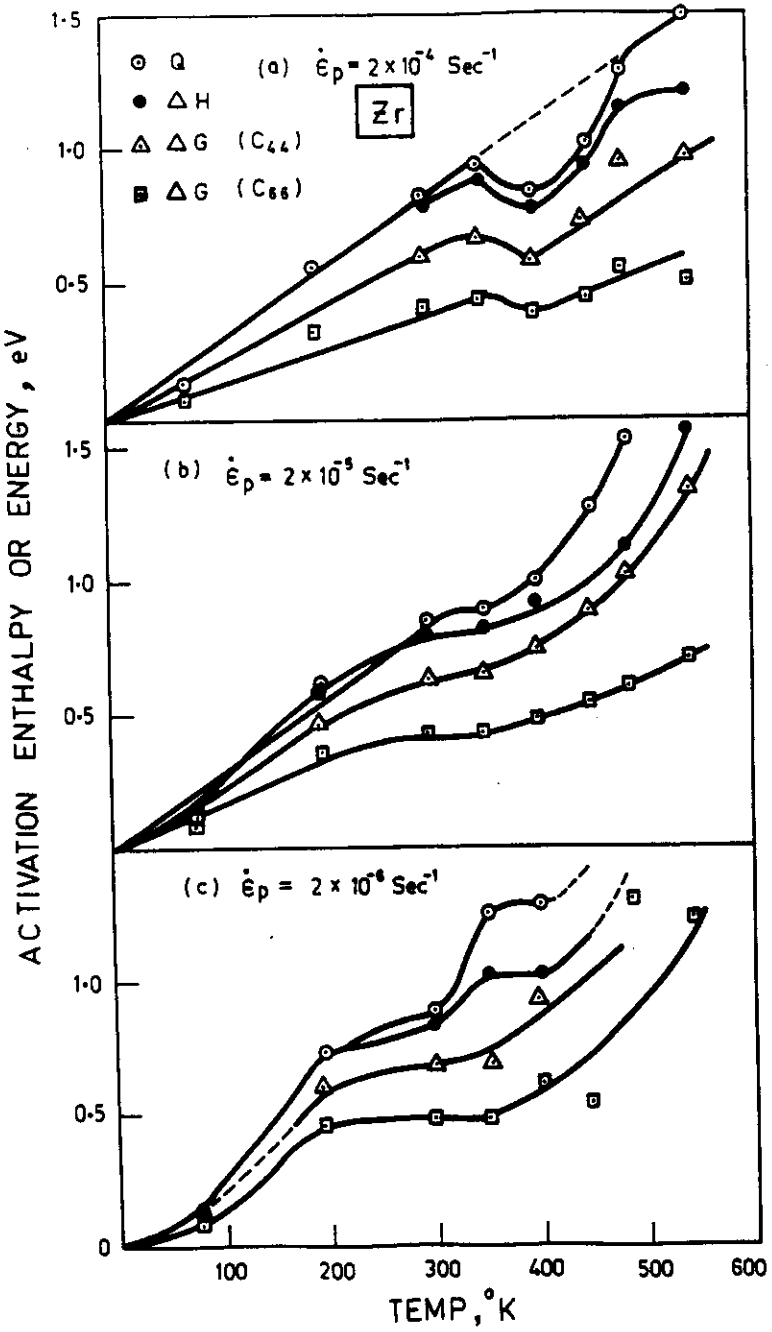

Fig. 6. Activation energy vs Temperature for Zr from TS experiments [Ref. 17].

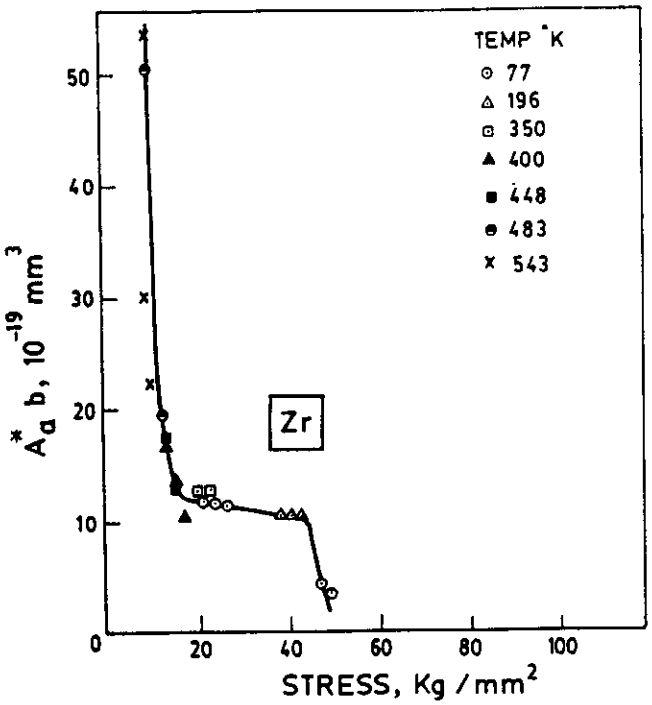

Fig. 7. Activation areas evaluated from TS experiments plotted against stress [Ref. 17].

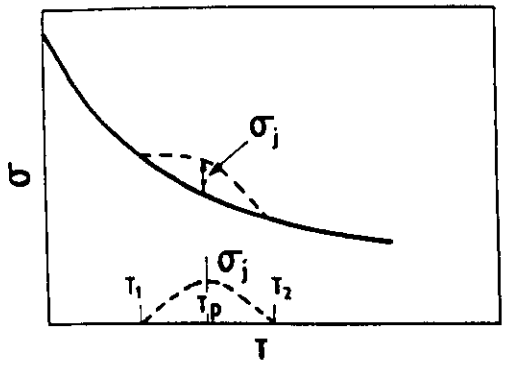

Fig. 8. (a) Schematic illustration of the influence of dynamic strain ageing on the flow stress vs temperature variation; full curve is the variation in the absence of dynamic strain ageing and the dotted curves indicate the contribution σ_j from strain ageing [Ref. 17,58].

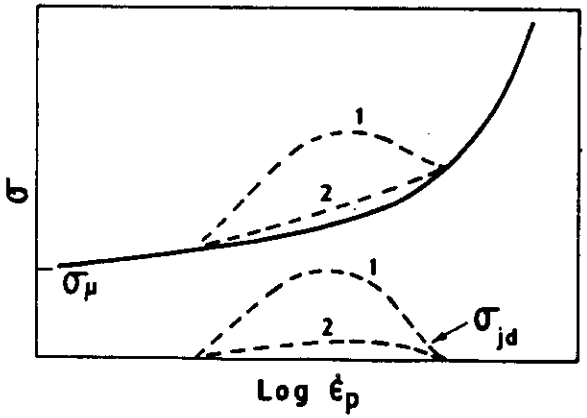

Fig. 8 (b) Schematic illustration showing the influence of dynamic strain ageing on stress - strain rate variation; 1 for the case of strong strain ageing and 2 for mild strain ageing [Ref. 17,58].

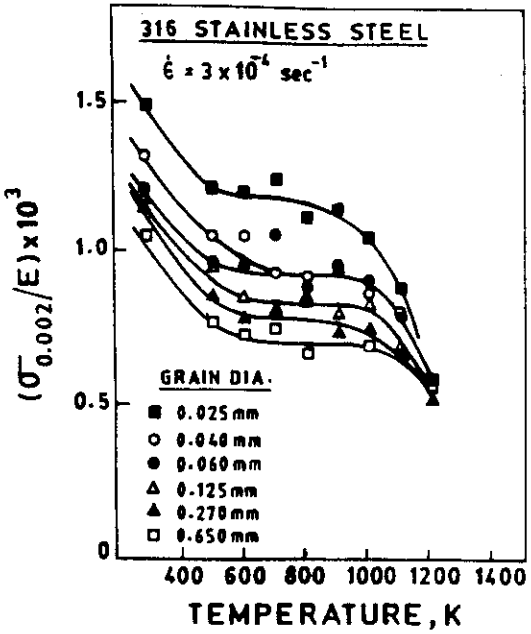

Fig. 9. Variation of yield stress with temperature for specimens of different grain sizes [Ref. 16,88].

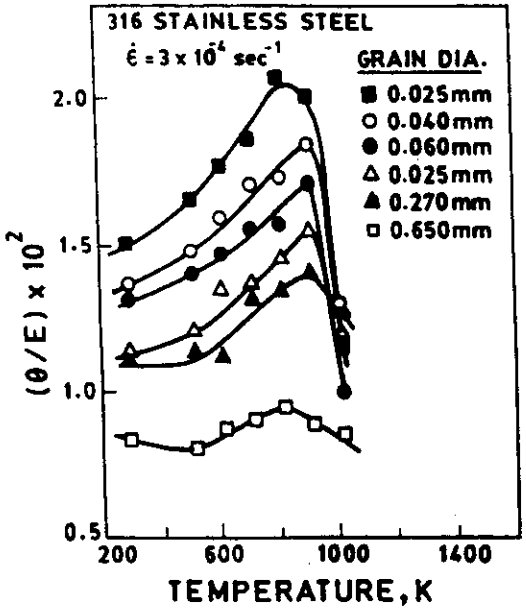

Fig. 10. Variation of work hardening rate with temperature for specimens of different grain sizes [Ref. 16,88].

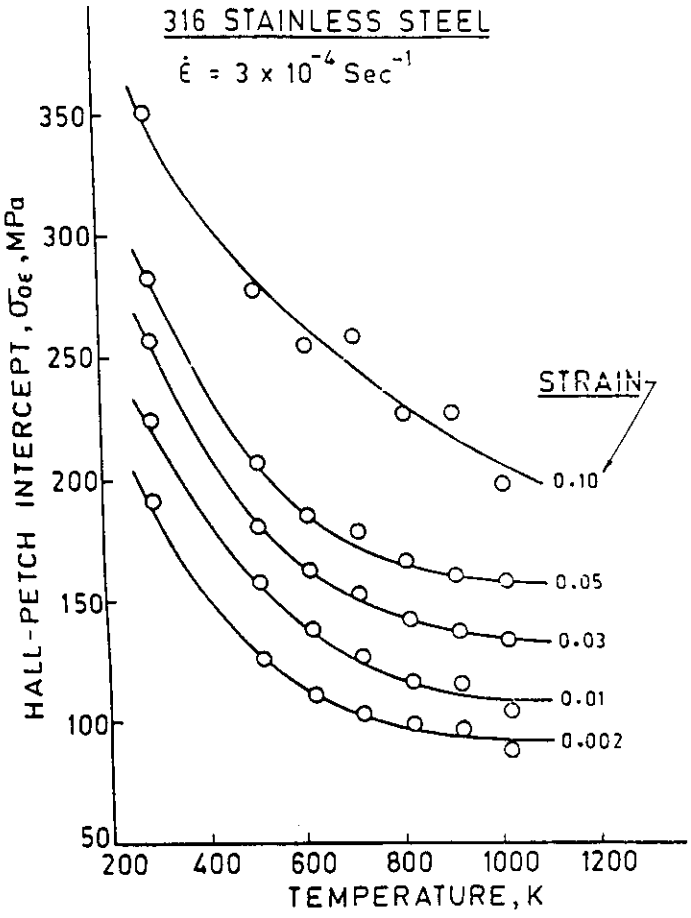

Fig. 11. Variation of Hall - Petch intercept with temperature at various strains [Ref. 16,88].

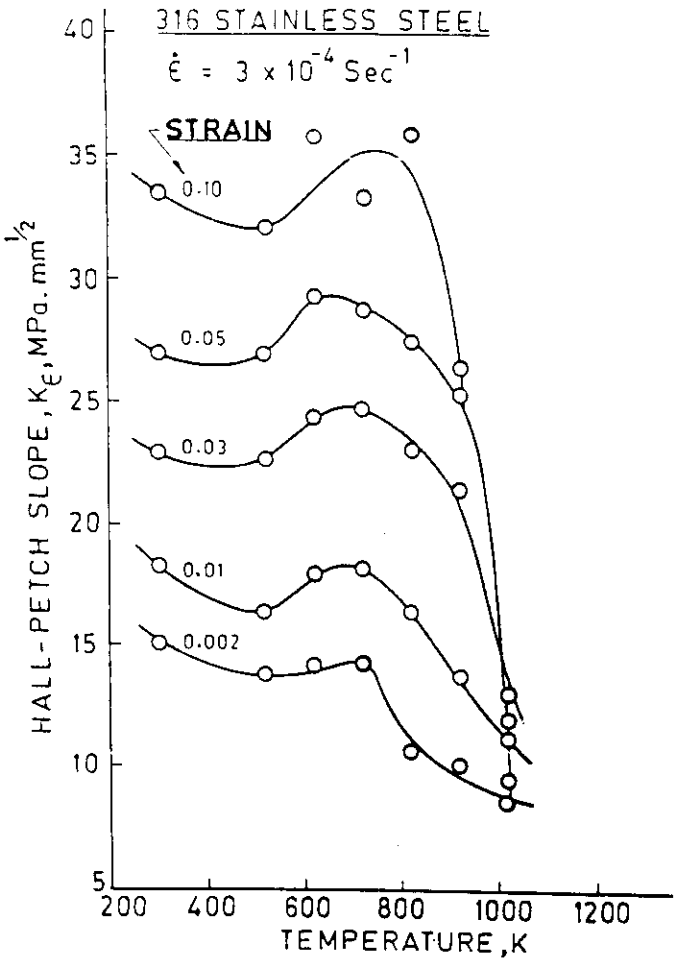

Fig. 12. Variation of Hall - Petch slope with temperature at various strains [Ref. 16,88].

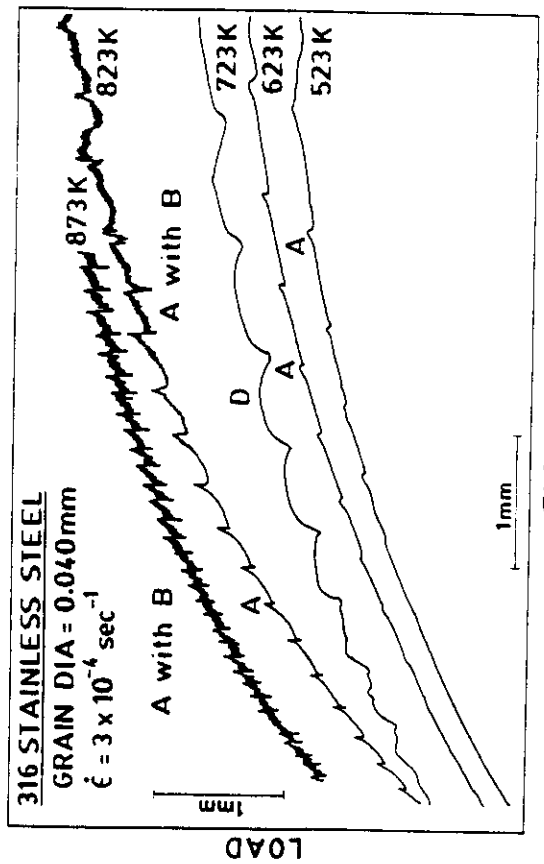

Fig. 13. Typical load - elongation curves in serrated flow range at different temperatures for specimens of grain size 0.040mm [Ref. 16,87].

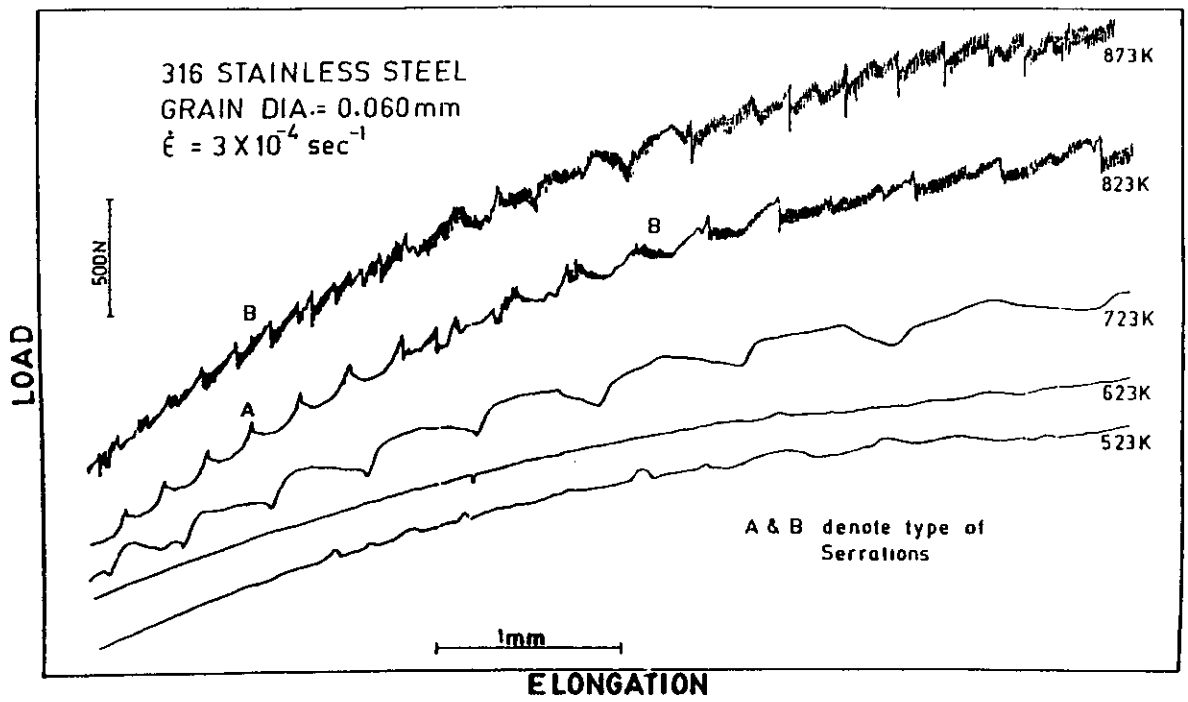

Fig. 14. Typical load - elongation curves in serrated flow range at different temperatures for specimens of grain size 0.060mm (Ref. 16,87).

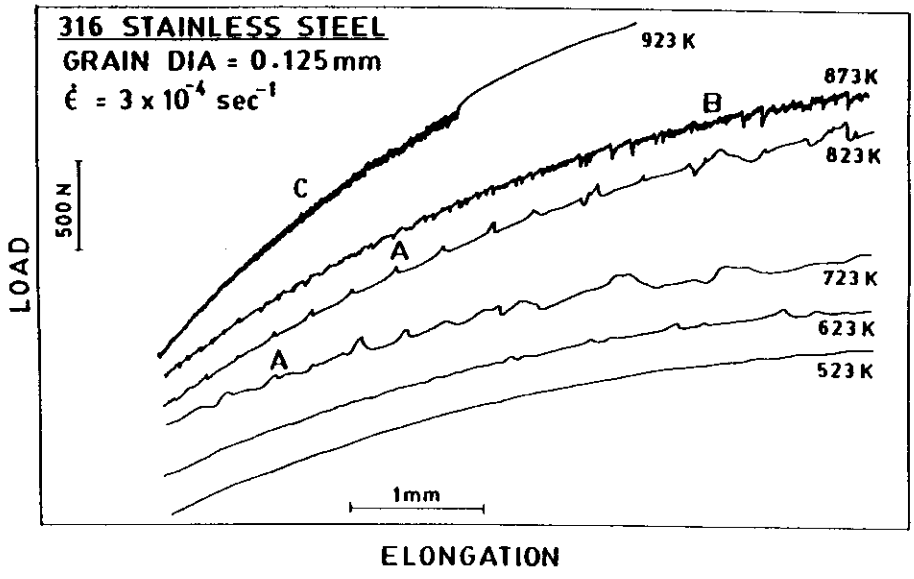

Fig. 15. Typical load - elongation curves in serrated flow range at different temperatures for specimens of grain size 0.125mm (Ref. 16,87).

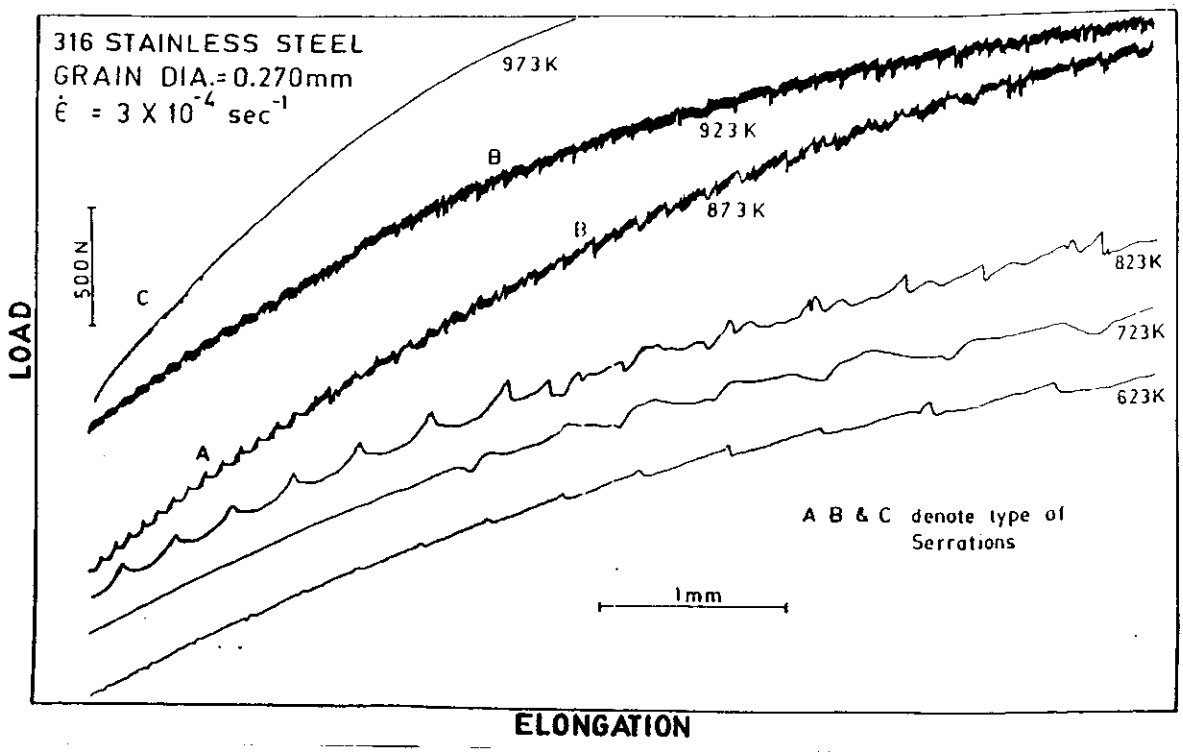

Fig. 16. Typical load - elongation curves in serrated flow range at different temperatures for specimens of grain size 0.270mm [Ref. 16,87].

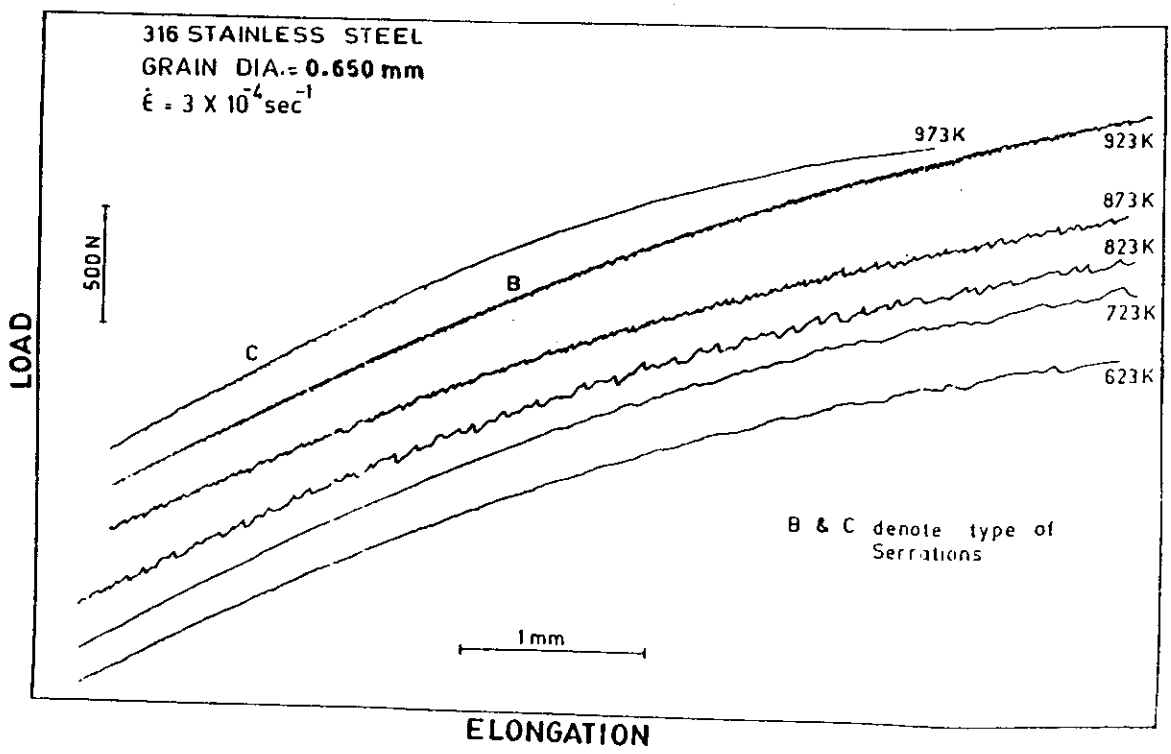

Fig. 17. Typical load - elongation curves in serrated flow range at different temperatures for specimens of grain size 0.650mm [Ref. 16,87].

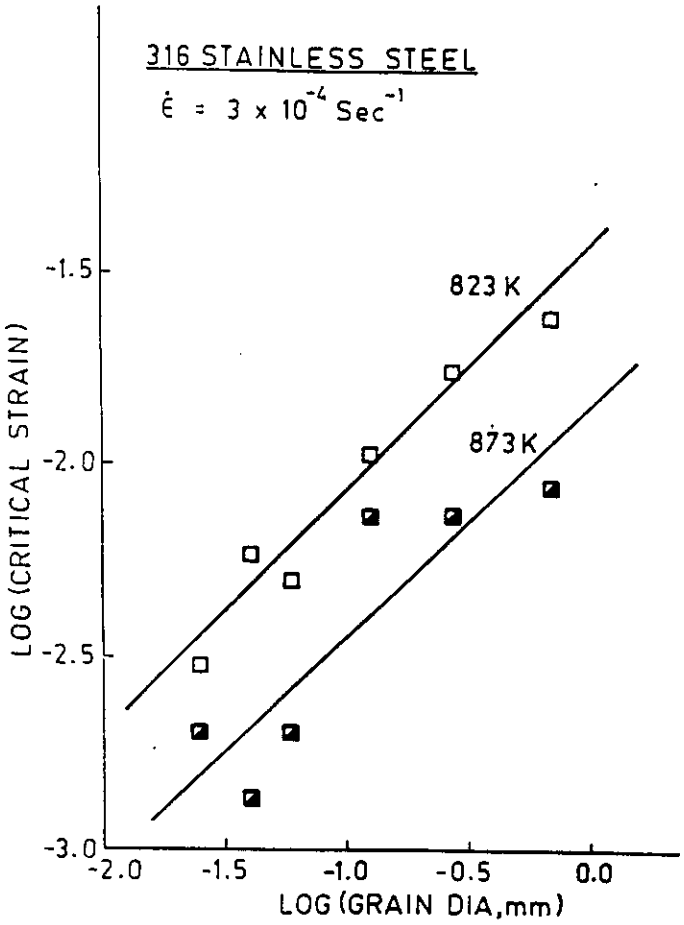

Fig. 18. Plots of log critical strain vs log grain size for specimens deformed at 823 K and 873 K [Ref. 16,87].

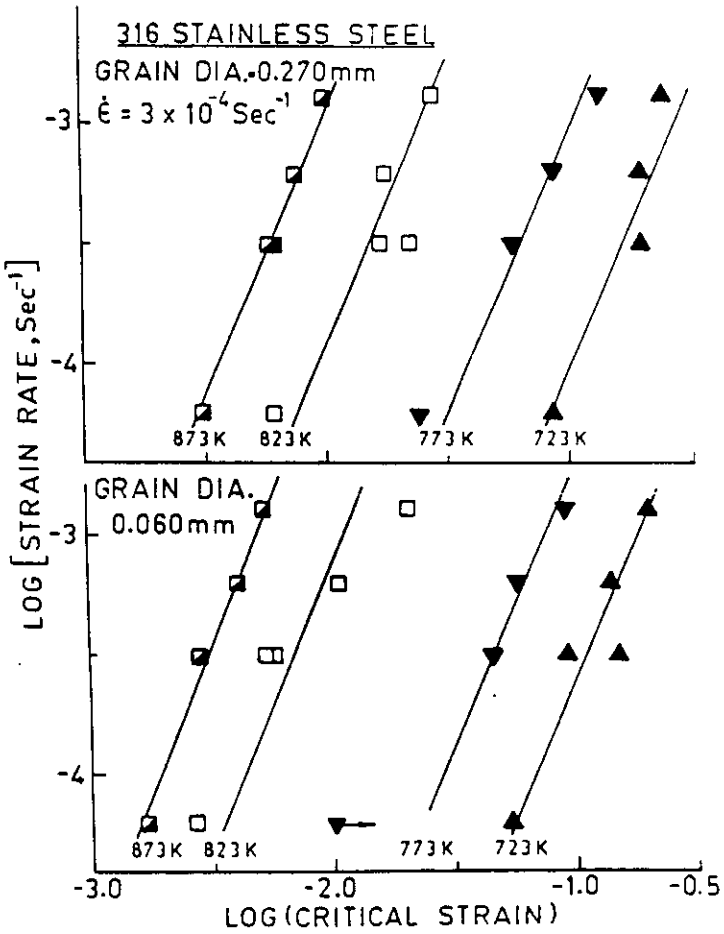

Fig. 19. Plots of log strain rate vs log critical strain for coarse (0.270mm) and fine (0.060mm) grained specimens deformed at different temperatures [Ref. 16,87].

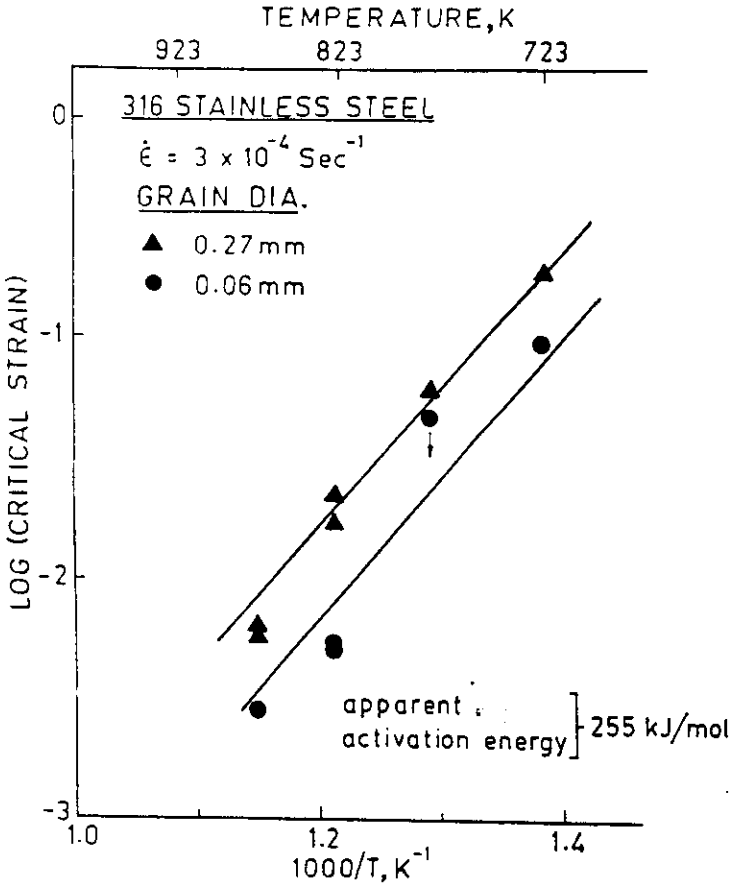

Fig. 20. Plots of log critical strain vs 1000/T for coarse (0.270mm) and fine (0.060mm) grained specimens [Ref. 16,87].

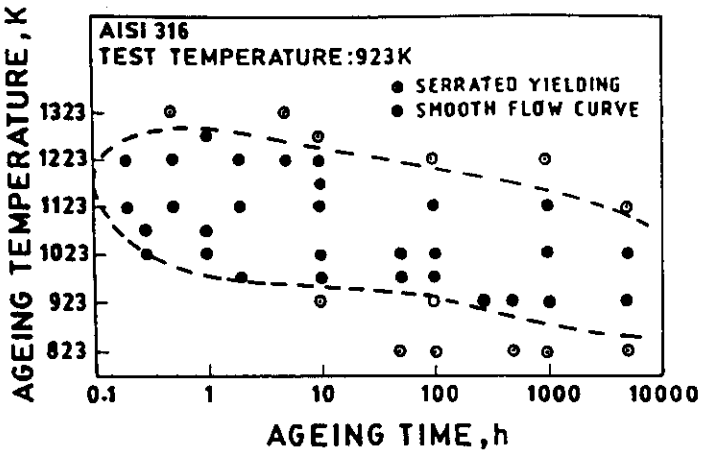

Fig. 21. Ageing temperature and time relationship of serrated yielding at 923 K [Ref. 98].

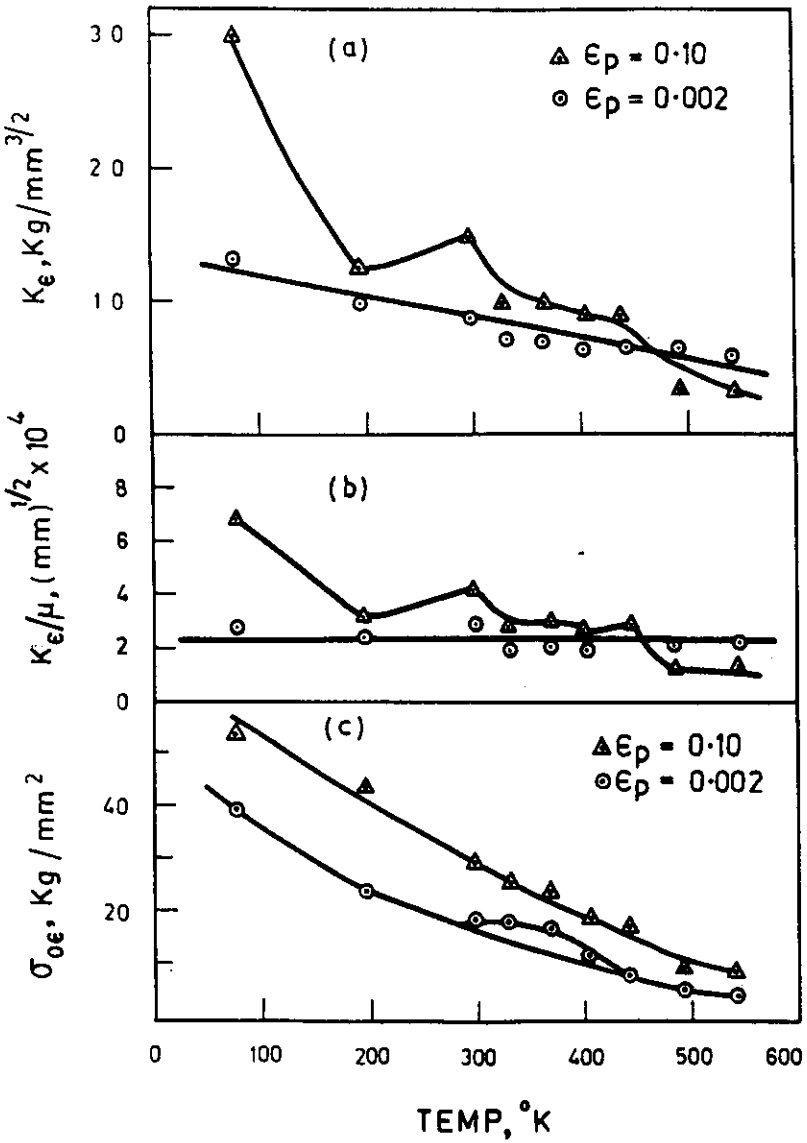

Fig. 22. Variation of K_ϵ, K_ϵ/μ and $\sigma_{0\epsilon}$ with temperature [Ref. 17].